RSC Applied Interfaces

ROYAL SOCIETY OF CHEMISTRY

REVIEW

View Article Online
View Journal

Cite this: DOI: 10.1039/d5lf00363f

Titanium and titanium compounds in the bipolar plate/gas diffusion layer system of polymer electrolyte membrane fuel cells: manufacturing methods, surface treatments and properties

Ermete Antolini

Titanium (Ti) is widely distributed in the Earth's crust in the oxide form. The two main properties of Ti are high corrosion resistance and strength-to-density, the highest of any metallic element. Ti and Ti compounds are widely used in polymer electrolyte membrane fuel cells (PEMFCs), playing various roles. In this review, the utilization of titanium and titanium compounds in the bipolar plate/gas diffusion layer system of PEMFCs is presented and discussed as well as the manufacturing methods and surface treatments, with particular attention to the corrosion resistance and the interfacial contact resistance. The aim of this work is to highlight that titanium can effectively replace the commonly used bipolar plate (BP) materials, such as graphite and stainless steel, and gas diffusion layer (GDL) carbon-based materials. The key findings are the new manufacturing methods of BP and GDL materials and the high corrosion resistance and low interfacial contact resistance of coated Ti BPs. The value of the key parameters of coated Ti, that is, the corrosion current density (I_{corr}) and the interfacial contact resistance (ICR), meeting DOE requirements, make Ti a highly competitive material suitable for its use as BP material. The use of carbon-free integrated Ti-based BP/GDL systems formed by Ti BPs, either uncoated or coated by Ti compounds, and Ti GDL is a key point that is to be developed. It should be noted that the use of Ti as BP material is only partially discussed in previous reviews, but there are no reviews that analyze in depth the use of Ti both as BP and GDL material like this one.

Received 18th November 2025,
Accepted 23rd December 2025

DOI: 10.1039/d5lf00363f

rsc.li/RSCApplInter

1. Introduction

Polymer electrolyte membrane fuel cells (PEMFCs) deliver high power density and present advantages, such as low weight and volume, low operating temperature (around 80 °C), short start-up time, and fast response to load fluctuations, compared with other types of fuel cells.[1] Direct methanol fuel cells (DMFCs) are similar to PEMFCS; however, they are powered by a methanol/water mixture directly fed to the fuel cell anode. The main components of a PEMFC/DMFC are the membrane electrode assembly (MEA) and the bipolar plates (BPs). The MEA consists of a proton/anion exchange membrane, a gas diffusion layer (GDL) and a catalyst layer (CL), as shown in Fig. 1a.[1] Both the electrodes of a fuel cell comprise the BP, the GDL and the CL (see Fig. 1b for the cathode). Bipolar plates are key components of the PEMFC stack. They uniformly disperse the reaction gas from the outside to the active sites on the surface area and remove the product formed by the reaction to the outside. The BPs are formed by lands and channels (Fig. 1b). The lands conduct the current and the channels distribute the reactant gas. As a consequence, the GDL in the electrode is also formed by channels and lands, placed on the channel and land of the BP, respectively.[2] The GDL is placed between the BP and the CL. The GDL uniformly diffuses the reaction gas from the BP to the CL. Moreover, it transports the electrons and removes heat produced by the reaction. Reactant gas diffuses in the channels through the GDL to reach the CL. The fuel cell performance remarkably depends on the mass transfer of reactants and products, in turn depending on the flow field of the BPs and the GDL. Thus, the optimization of the BPs and the GDL is a key point in order to effectively supply reactants and remove products.[3] The BP/GDL interface is critical, determining the contact resistance for electron and heat transport. Moreover, this interface can also act as a pooling location for liquid water due to an imperfect contact between the BP and the GDL surface, affecting H_2O distribution in the GDL and leading to mass transport losses.[4]

Titanium (Ti) is one of the most abundant elements in the world. The two most useful properties of Ti are high corrosion resistance and strength-to-density, the highest of any metallic element. In its unalloyed form, Ti is as strong as some steels, but less dense.[5]

Scuola Scienza Mareriali, Cogoleto, Genova, Italy. E-mail: ermantol@libero.it

The high corrosion resistance of Ti is due to the formation of a thin oxide layer acting as a shield against corrosion. Bare Ti and Ti compounds can play many roles in the BP/GDL system, such as substrate and coating for BPs, and gas diffusion backing (GDB) and hydrophilic layer (HL) for the GDL layer. In this work, the application of titanium and titanium compounds in the BP/GDL system of PEMFCs is overviewed and discussed as well as the manufacturing methods and surface treatments, with particular attention to the corrosion current density (I_{corr}) and the interfacial contact resistance (ICR). The objective of this review is to demonstrate that titanium can be a valid substitute of the commonly used BP materials, such as graphite and stainless steel, and carbon-based materials for the GDL. The key findings are the new manufacturing methods of BP and GDL, and the high corrosion resistance and low interfacial contact resistance of coated Ti BPs provide a good support for this thesis The use of carbon-free integrated Ti-based BP/GDL systems formed by Ti BPs, either uncoated or coated by Ti compounds, and Ti GDL is a key point to be developed. While other reviews focused on the use of graphite and metallic materials, including Ti, as BPs, this work is the only one entirely addressed to the use of Ti as BP material, including the integrated use of Ti BP and Ti GDL.

2. Titanium bipolar plates

As previously reported, bipolar plates serve many functions, such as reactant gas distribution, current conduction and heat removal from the acting area. BPs comprise *ca.* 70–80% of the weight, the greatest part of the volume and *ca.* 30–50% of the price of the fuel cell stack; thus, both BP weight and volume reduction will impact directly on the cost reduction.[6] Currently, the base materials for BPs overall include graphite, metals and composite materials.[7] Graphite, having outstanding electrical conductivity and corrosion resistance, has been widely utilized as a BP material. Despite that, difficulties in manufacturing graphite into fine flow channels result in a high cost of the process, hindering its commercial applications.[7] The ease of manufacturing, high electrical and thermal conductivity and low cost make metals promising candidates to replace graphite as PEMFC bipolar plates.[8] Among metals, stainless steel (SS) is the most studied. A disadvantage, however, is its inclination to corrosion under PEMFC conditions together with the release of ions that may contaminate the membrane. Titanium, although it is more expensive than SS, presents the advantages of higher corrosion resistance, lighter weight and higher strength. Its low density (*ca.* 60% than that of SS) allows decreasing the mass and volume of the bipolar plates. However, the passivation film formed on the Ti surface, which gives rise to the high corrosion resistance, leads to a remarkable enhancement of the interfacial contact resistance. Moreover, F^- ions in the PEMFC environment can give rise to pitting corrosion, decreasing PEMFC durability. These drawbacks can be solved either by coating the titanium surface with suitable materials, combining corrosion resistance and conductivity, or by using Ti alloys as BP substrates. Moreover, titanium processing is difficult, overall because of its high strength and high melting point, posing challenges for machining. The commonly used machining methods contribute to the significantly higher manufacturing costs of titanium BPs; thus, new and cost-effective forming methods have been explored. Among them, additive manufacturing is a reasonable less expensive alternative to commonly used machining manufacturing methods to fabricate titanium BPs.

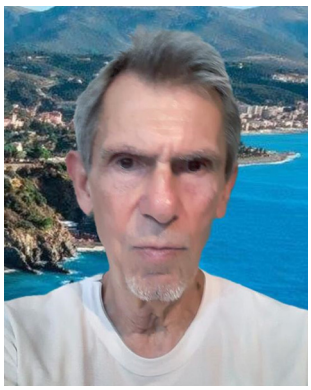

Ermete Antolini

Ermete Antolini received his PhD in Chemistry from the University of Genova, Italy. He worked at Ansaldo Ricerche, Genova, Italy, ENEA, Roma, Italy and Scuola Scienza Materiali, Genova, Italy. He was a visiting professor at Ecole National de Chimie, Paris, France (1999) and at Institute of Chemistry of USP, Sao Carlos, Brazil (2001–2010). He has over 160 scientific publications with more than 19 000 total citations and an H-index of 68 (GoogleScholar). He was recognized as a Highly Cited Researcher 2014 by Thomson Reuters (ISI Web of Knowledge) and was in the World's Top 2% Scientists list (2020), the first of Italians in the Enabling & Strategic Technologies field and in the Energy subfield. He is a member of the Editorial Boards of Applied Catalysis B: Environmental and Catalysts. His research interests focus on the development of materials for heterogeneous catalysis with emphasis on fuel cell catalysts.

2.1. Titanium bipolar plate manufacturing methods

A representative metallic BP and the micro flow channels are shown in Fig. 2.[9] The main parameters of the channels are channel depth and width, rib width, fillet radius, draft angle and channel/plate thickness. The fuel cell performance tightly depends on BP parameters, such as the channel depth, the aspect ratio (the channel depth-to-the channel width ratio) and the thinning rate in the thickness direction.[9] To improve fuel cell performance and duration, it is mandatory to increase the channel depth and aspect ratio of metallic BPs and to decrease the reduction in the plate thickness after forming. A drawback of titanium BPs is the poor formability at room temperature (RT).[10] Indeed, Ti has low ductility and large springback due to the hexagonal close-packed (HCP) crystal structure.[11] The commonly used manufacturing methods, such as stamping and rubber pad forming (RPF), due to their ease of manufacturing and low cost, were used to fabricate Ti bipolar plates. Mahabunphachai *et al.*[12] prepared Grade 1 (softer) and Grade 2 (harder) Ti BPs by using a cold stamping process. The

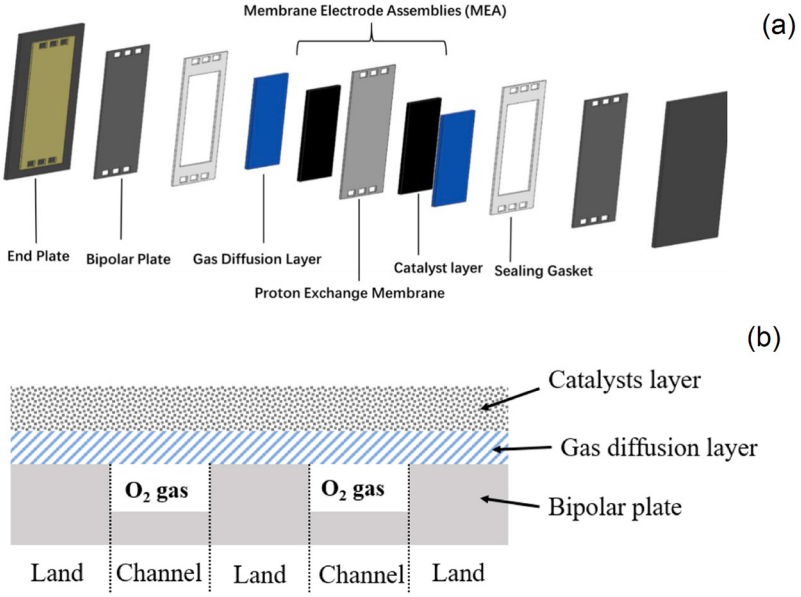

Fig. 1 (a) Schematic view of a typical PEMFC; (b) configuration of BP, GDL and CL in the PEMFC cathode. (a) Reproduced from ref. 1, copyright 2024, with permission from Elsevier, (b) reproduced from ref. 2, https://creativecommons.org/licenses/by/4.0/.

Grade 1 and Grade 2 Ti BPs showed low forming depths of 0.13 mm and 0.09 mm, respectively, with fracturing at 200 kN in the Grade 2 Ti BP. Kim *et al.*[13] utilized dynamic load stamping to fabricate Grade 5 (Ti-6Al-4 V) low-alloyed titanium BPs. Using this stamping method, channel depths of 0.251 and 0.353 mm were obtained, with a channel aspect ratio of 0.252 (depth of 0.353 mm). The low elongation rate of titanium gives rise to fractures for loads >100 kN, indicating that cold stamping is not suitable to form Ti BPs. According to Nakagaki,[14] an extension rate of 30% of Ti sheets cannot support the forming of precise microchannels. Jin *et al.*[15] and Lee *et al.*[16] utilized quasi-static drive rubber pad forming (QS-DRPF) to prepare Grade 5 Ti BPs with a channel aspect ratio of 0.3375 (depth of 0.27 mm, lower than 0.5 mm in SS BPs). The higher decrease of the performance with increasing current density for the PEMFC equipped with Ti bipolar plates than that with graphite BPs, however, could be ascribed to the oval shape of the Ti BP channels, resulting in a smaller contact area with the MEA. These commonly used methods are not satisfactory to obtain suitable Ti BPs for use in PEMFCs. Therefore, new and cost-effective forming methods have to be probed to enhance Ti formability. Several novel methods were proposed, such as hot stamping, ultrasonic-vibration-assisted stamping, electrohydraulic forming (EHF), multistage stamping, electromagnetic forming (EMF) and additive manufacturing (AD). Modanloo *et al.*[17] prepared titanium BPs by a warm stamping process. The maximum channel depth was 0.494 mm (forming rate of 65.87%) at 100 °C and 0.373 mm (forming rate of 49.74%) at RT. The thinning rates were 5% and 10% at RT and 100 °C, respectively. The inclination of Ti sheet to springback decreased with increasing forming temperature. By stamping at 100 °C, a Ti BP without curl was obtained. Wang *et al.*[18] evaluated an ultrasonic-vibration-assisted stamping method process for manufacturing Ti BPs. Among the vibration parameters, vibration power has the maximum influence on the depth, followed by the vibration interval time and the vibration duration time. In addition, the rolling direction will affect the channel depth. When the microchannels are parallel to the rolling direction, the depth of a microchannel

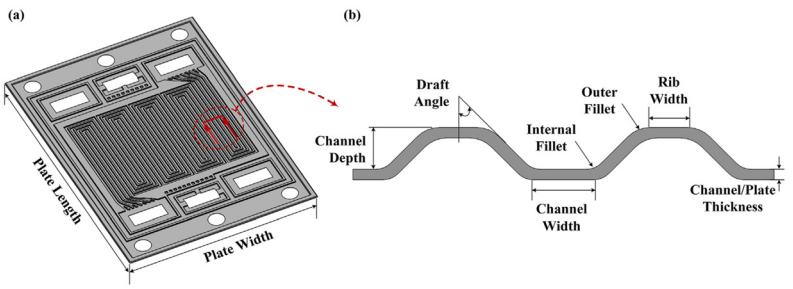

Fig. 2 Schematic diagram of a typical metallic BP: (a) overall; (b) cross section of the channels. Reproduced from ref. 9, copyright 2021, with permission from Elsevier.

was the largest. Compared to the stamping without ultrasonic vibration, the depth limit is increased from 285.5 μm to 311.5 μm using an ultrasonic power of 70%, interval time of 10 s, and duration of 1 s due to the acoustic softening effects. Pang *et al.*[19] proposed an electrohydraulic forming (EHF) method, taking advantage of high strain rate (HSR) deformation. By a comparative analysis of the forming between the conventional RPF and the EHF methods, they proved the technical feasibility and advantages of EHF for the manufacturing of Ti BPs.

The multistage forming process allows solving the drawbacks related to the use of single-stage forming. Xu *et al.*[20] investigated the suitability of the multistage forming process of titanium BPs. The limit forming depth of channels depended on the channel direction, with the greatest limit forming depth obtained when the channel and the rolling directions of Ti sheets are parallel. The channel depth increased from 0.438 to 0.621.0 mm, and the aspect ratio from 0.46 to 0.67, with respect to the single-stage forming method. The ICR values at different pressures between carbon paper and Ti BPs fabricated by single- and multistage forming processes are shown in Fig. 3. The ICR of the Ti BPs obtained by three-stage forming was lower than that of Ti BPs fabricated by the single-stage forming process. The bottom of channels of Ti BPs fabricated by three-stage forming had a greater contact area due to the improved aspect ratio and base angle. Thus, by using the multistage method, BPs with better accuracy can be fabricated, reducing the ICR between BPs and GDL. A multistage process was developed to form complicated geometries by dividing the process into three steps: preforming, intermediate annealing and final stamping. Zhang *et al.*[21] used this method to form Ti bipolar plates. Different rectangular samples were utilized for the forming process. First, ultrathin Ti sheets were stamped by a tool with a larger radius to shape the preform, avoiding strain localization. Then, preforms were annealed at 600 °C for 10 min. The annealed samples were stamped by a second tool to form the final shape. The scheme of the multistage process and the design of the target contours and tool geometries are shown in Fig. 4.

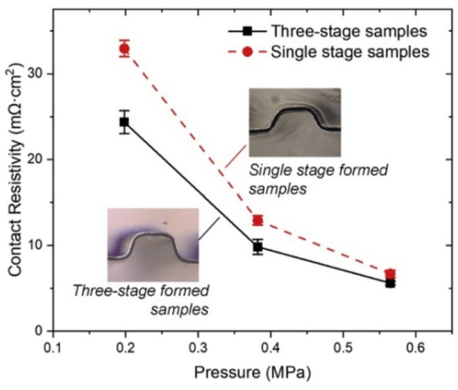

Fig. 3 ICR of the samples formed after three-stage and single-stage stamping processes. Reproduced from ref. 20, copyright 2021, with permission from Elsevier.

The preform annealing method enhances the thickness uniformity and forming limit of Ti sheets, improving BP formability. Intermediate annealing at 600 °C decreased the twin area fraction and the low-angle grain boundaries (LAGBs) amount in the preformed Ti sheet, leading to an increase of total elongation from 36% to 41% and an enhancement of both thickness uniformity and channel forming limit than the RT two-stage stamping method. Because of this, flow channels with a high aspect ratio of 0.79 and a narrow wall angle of 5° were obtained on Ti sheets. Xie *et al.*[22] utilized a three-stage process to form Ti BPs. Better high aspect ratio, fine channel structure, and uniform channel wall thickness were observed by utilizing the three-stage forming method compared to the single-stage forming method. The channel obtained by the three-stage forming process was deeper than that by the single-stage process. To increase the channel depth, the punch displacement has to be enhanced during the first- and second-stage forming processes. The channel depth increased by 31 μm with respect to the single-step forming. Finite element (FE) simulation results indicated that thickness reduction from 47% to 22% can be achieved by the arc design of the punch end in the first stage, in good agreement with experimental measurements.[23] The optimum rib-to-channel width ratio was 0.4–0.6, with a final channel corner radius of 0.15 mm. The uniform small grain size improved the characteristics of BPs for their use in PEMFCs. Titanium sheets are inclined to springback during stamping, affecting forming precision. The influence of grain size, orientation and forming angle on the micro-bending springback behavior of Ti sheets was evaluated by experimental measurements and theoretical calculations.[24] Experimental measurements indicated that the springback angle first decreases and then increases with increasing grain size. The forming angle has a nonlinear effect on the springback angle. The springback angle increases with increasing the angle, but the rate of increase depends on the proportion of plastic and elastic strains. At small bending angles, the proportion of plastic strain is high, decreasing springback. At larger forming angles, the proportion of elastic strain increases, resulting in an increased springback. The prediction of the springback behavior by theoretical calculations was in good agreement with experimental measurements. A multi-step roll forming method was proposed by Zhang *et al.*[25] With respect to single-step roll forming, the multi-step roll forming decreases both the maximum thinning rate by nearly 5% and the true strain in fillets by more than 22%. Compared to the stamping method, multi-step roll forming presented better thickness uniformity, and the maximum thinning rate was *ca.* 4% lower.

EMF is a high-speed forming method utilizing a pulsed magnetic field that remarkably enhances sheet metal formability, reduces springback, and suppresses wrinkling, making it suitable for manufacturing Ti bipolar plates.[26] Various studies reported the use of EMF to form Ti sheets:[27–29] EMF can

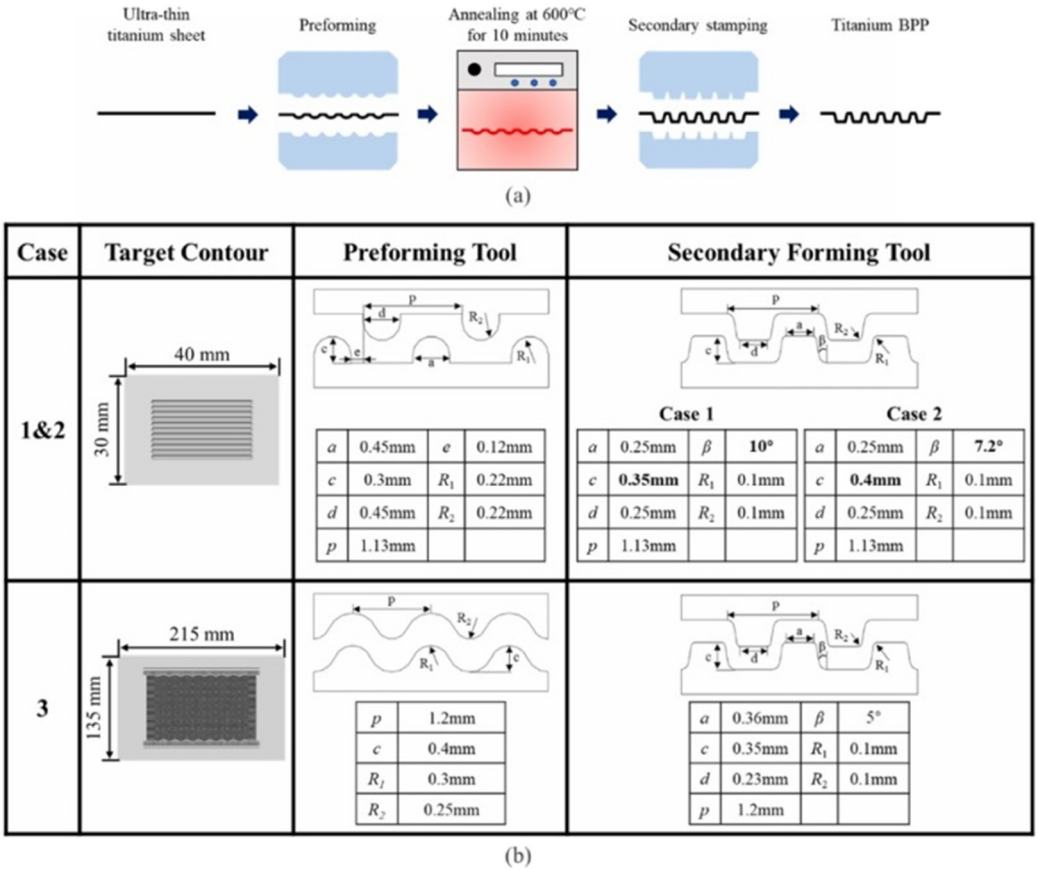

Fig. 4 (a) Schematic diagram of the multistage process and (b) design of the target contours and tool geometries for three cases. Reproduced from ref. 21, copyright 2024, with permission from Elsevier.

remarkably enhance the ultimate strength and Ti forming limit, indicating that the EMF technology has high potential in Ti bipolar plate forming. A uniform distribution of pressure is necessary to obtain suitable BPs. The spatial distribution of the forming pressure is controlled by the actuator configuration. Conventional electromagnetic actuators are flat spirals that generate a non-uniform pressure distribution. A new electromagnetic actuator, the uniform pressure actuator (UPA), was proposed by Kamal and Daehn.[30] EMF can remarkably reduce the BP thinning rate in the thickness direction, and UPA can enhance the uniformity of the channel depth. Wang and Wang[31] used EMF with a UPA to form a 0.08 mm Grade 2 Ti BP with a channel aspect ratio of 0.22 and a channel depth of only 0.176 mm (*ca.* 54% of full channel depth). Wu *et al.*[32] used a new type of UPA formed by an external coil and an internal closed circuit. A Ti BP with 0.294 mm channel depth was obtained, with some channel depth deviation (5.97%), still far from the proper channel depth of 0.4 mm. Dong *et al.*[9] fabricated titanium BPs by EMF with a UPA coil. Simulation results by a three-dimensional coupled electromagnetic–mechanical model showed that the channel depth depends on the impact velocity of the Ti workpiece. Ti BPs with proper channel depth (0.4 mm), high aspect ratio (0.67) and low thinning rate (<15.89%) were formed at a velocity of 286 m s^{-1}, attesting that EMF is a suitable method to fabricate titanium BPs. Wang *et al.*[33] utilized a multiphysics EMF analysis model to optimize the geometric shape of an arc-shaped UPA. On the basis of the theoretical results, TA1 titanium BPs with a channel depth of 0.4 mm, an aspect ratio of 0.53, a maximum thinning rate of 18.2% and a channel filling rate >95% were obtained. The formability of Ti BPs was investigated using QS, EM, and EM-QS forming methods.[34] For the QS forming method, the depths of the channels on the BP increased with the applied load, with the formation of small cracks at a depth of 0.719 mm at 25.5 kN. For the EM forming method, the channel depth increased with the discharge voltage, and small cracks were formed at 12 kV, with a limit channel depth of 0.711 mm. The maximum channel depth deviation was 6 μm for QS stamping, whereas it was 31 μm for EM stamping. For the EM-QS two-step stamping with different EM discharge voltages, the channel depth increased with increasing discharge voltage up to a maximum of 0.879 mm at a discharge voltage of 10 kV. The sample with a grain size of 15.5 μm achieved the maximum channel depth. The maximum channel depth deviation was 8 μm due to the subsequent QS stamping. Thus, the EMPB-QS stamping method not only can enhance the channel depth of BP but also allows one to obtain a good channel-depth uniformity. In a conventional EMF, the low conductivity of Ti needs the utilization of a highly conductive driver sheet, limiting a further enhancement of BP formability. Thus, Wu *et al.*[35] introduced an

innovative EMF process with independent loading of the magnetic field and current (EMF-ILMFC). The dynamic deformation of TA1 was studied using QS, electromagnetic bulging with driver sheets (EMB-DS), and electromagnetic bulging with the new method (EMB-ILMFC). The results indicated that the forming limit using EMB-ILMFC was remarkably higher than that using the other methods, with a maximum enhancement of 139.1%. Theoretical and experimental results showed that thermal effects reduced flow stress and extended the duration of high strain rates, improving Ti formability during dynamic deformation.

Additive manufacturing (AM) is a process based on adding materials layer by layer to fabricate three-dimensional (3D) objects directly through the use of computer-aided design (CAD) models. Some studies have optimized the design of BPs through the use of this 3D-printed technique. Gould *et al.*[36] used the 3D-printing direct metal laser sintering (DMLS) process to fabricate 21 cm^2 Ti-alloy BPs with embedded flow channels. The performance of a single PEMFC with coated 3D printed BPs was close to that of the cell with graphite BPs. However, a 40-cell stack with 3D-printed BPs showed a lower current density at 0.6 V than the expected value due to the high ICR by distortions from flatness in the 3D-printed BPs. The surface roughness of the DMLS BP was 7.6 μm. As the GDL surface roughness was as high as 24.5 μm, it resulted in a high ICR. By polishing the BPs to a roughness of 1.6 μm, the BP/GDL contact remarkably increased, reducing the ICR.[37] Piri *et al.*[38] compared different 3D-printed BPs, manufactured by PolyJet 3D printing, stereolithographic apparatus (SLA) 3D printing and laser-cutter technologies. SLA BPs showed the best results in terms of the pressure drop and velocity profiles. Celik *et al.*[39] compared the performance of PMFCs with SS, gold-coated AM Ti and machined graphite with the same flow field geometry as the bipolar plates. The cell with 450 nm gold coated AM titanium BPs delivered the highest maximum power density (MPD) (639 mW cm^{-2}), whereas the MPD of the PEMFCs with graphite and SS BP was only 322 mW cm^{-2} and 173 mW cm^{-2}, respectively. Advanced AM techniques, in particular laser powder bed fusion (LPBF), were used to fabricate Ti lattice structures with specific porosity and morphology. Heydari *et al.*[40] fabricated porous Ti BPs by LPBF utilizing a Kelvin cell lattice. The optimal Ti lattice, with 1 mm cell size, 125 μm ligament, and 1 mm thickness, delivered a 30% higher power density and a 60% higher limiting current than a commonly used serpentine graphite flow field.

Summarizing, low-cost and easily manufactured techniques, such as stamping and rubber pad forming, were used to fabricate Ti BPs. These established techniques, however, are not technically satisfactory to obtain suitable Ti BPs for use in PEMFCs. Therefore, new and cost-effective forming methods have to be probed to enhance Ti formability. The most promising novel methods are multistage stamping, electromagnetic forming and 3D-printed technique. Suitable BPs have been obtained by using these methods, but they have some technicalities and need to be fine-tuned. For example, a drawback of the 3D technique used to fabricate Ti BPs is the increase of the contact resistance caused by deleterious distortions from flatness in the BPs [Gould]. Such flatness deviations might be accommodated for testing single-cell fuel cell flow field designs. This is not a drawback for testing single-cell BP designs, where end plates can be tightened to accommodate the non-uniformities, or matching BPs can be selected from a larger batch. However, the lack of flatness is a problem when 10s of BPs are stacked in series, thus limiting the present 3D technology to single-cell testing only or small short stacks.

Literature data on some titanium BP parameters (channel length and aspect ratio) from different manufacturing methods are reported in Table 1.

2.2. Coatings and coating techniques for titanium bipolar plates

A BP must have both high corrosion resistance and low interfacial contact resistance. Although the passive film on

Table 1 Literature data on some titanium BP parameters (channel length and aspect ratio) from different manufacturing methods

Manufacturing method	Channel depth/mm	Aspect ratio	Reference
Cold stamping	0.13 (Ti G1), 0.08 (Ti G2)	—	12
	0.25 (die curvature 0.1 mm)	—	13
	0.35 (die curvature 0.3 mm)	0.252	
Rubber pad forming	0.27 (channel draft angle 30°)	0.338	15, 16
Warm stamping	0.49 (100 °C), 0.37 (RT)		17
Ultrasonic-vibration-assisted stamping	0.312		19
Three-stage stamping	0.62	0.67	20
	—	0.79	21
	0.407	—	22
Electromagnetic forming (uniform pressure actuator)	0.176	0.22	31
	0.294	—	32
	0.4	0.67	9
	0.4	0.53	33
	0.711 (12 kV)	—	34
EM-QS	0.879		34
Additive manufacturing	0.27	—	39
	0.25 (after Au coating)	—	

the Ti surface protects it from corrosion, it is also an electrical insulator, reducing cell performance. Moreover, it increases the ICR between BPs and GDL. The most common way to reduce these drawbacks is surface modification with conductive and highly corrosion-resistant coatings. In addition, coatings must have a sufficiently high water contact angle (CA) to remove water and avoid flooding. First, Wang *et al.* proposed three different types of titanium surface modification: titanium sintering with IrO_2[41] and titanium coating with Pt[50] and gold.[42] These materials are electrically conductive and have good mechanical properties. PEMFCs with these surface-modified Ti bipolar plates delivered very high power densities. These noble metals have outstanding corrosion resistance but form unstable oxides and are expensive; thus, more suitable and cheaper materials have to be used to coat Ti bipolar plates.

2.2.1. TiN coatings. Ti-based ceramics, such as TiC and TiN, with high corrosion resistance and electrical conductivity, were proposed as low-cost coatings for Ti bipolar plates.[15,43] TiN and Ti have a thermal expansion coefficient that differs by 0.63%, much lower compared to that between TiC and Ti (17.74%). Thus, TiN is more suitable than TiC as a coating for titanium BPs. Moreover, the high compatibility of TiN with Ti (higher than with SS) facilitates the formation of tight coating bound to the titanium substrate. Plasma nitriding (PN) is a largely utilized chemical heat treatment process. Compared with the physical vapor deposition (PVD) method, PN is a cost-effective and simple way to coat the BP surface and does not present the drawback of peeling of the coating owing to poor adhesion. In this case the presence of an interface between the surface layer and the substrate is not observed, as N atoms diffuse into the substrate and react with titanium to form the coating. Moreover, the formation pinholes can be quite avoided. On these bases, different studies reported the formation of a protective nitride layer, commonly TiN, by PN of Ti bipolar plates.[44–47] Generally, PN improves corrosion resistance and decreases the ICR of titanium BPs. However, when the PN process is performed at high temperatures (900–1100 °C) above the phase transformation temperature of α-Ti to β-Ti, deformation of the Ti workpiece can occur. Furthermore, cracks formed in the TiN film observed by Liu *et al.*[44] were attributed to the thermal expansion mismatch between TiN and the Ti substrate during cooling from 900 °C. Thus, the TiN coating obtained by PN of titanium at 900 °C did not enhance Ti corrosion resistance.[44] To overcome the drawbacks related to PN at high temperatures, Shen and Wang[46] carried out PN at a lower temperature. PN of titanium was carried out at 700 °C for various times in an ammonia atmosphere. With increasing process time, an enhancement of both conductivity and corrosion resistance of Ti BPs was observed due to the formation of a dense Ti_2N layer. Jin *et al.*[47] utilized liquid phase plasma electrolytic nitridation to coat the Ti-6Al-4 V (TC4) alloy. The electrolytic solution used for the liquid phase PN was composed of CH_4NO_2, KCl and deionized water. CH_4NO_2 was the nitrogen source and KCl the conductive agent. Higher CH_4NO_2 concentration tends to form a more compact structure. The coating with 600 g L^{-1} CH_4NO_2 showed the lowest I_{corr} and the highest corrosion resistance. Different techniques other than PN were also utilized to coat titanium BPs with a TiN layer, such as reactive magnetron sputtering (RMS) and multi-arc ion-plating (MIP). RMS is a PVD technique based on sputtering a target material with a reactive gas, such as nitrogen, to form thin films like nitrides. For example, TiN can be formed by sputtering a Ti target with N. Jin *et al.*[15] coated titanium BPs with a TiN layer formed by RMS. Fig. 5 shows the polarization curves of the PEMFCs with graphite BPs and bare and TiN-coated Ti BPs. The PEMFC with TiN-coated titanium BPs delivered a better performance than the cell with the uncoated one, close to that of the cell with graphite BPs.

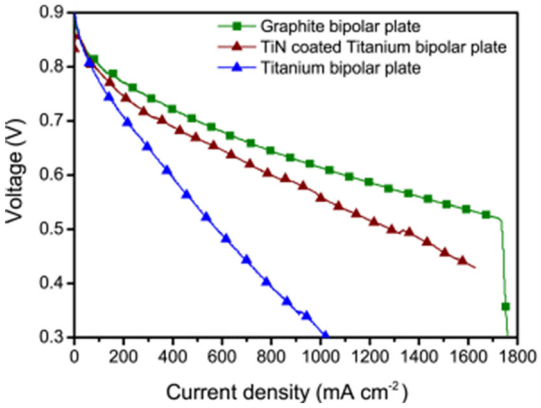

Fig. 5 Polarization curves for single PEMFCs with uncoated titanium, TiN-coated titanium and graphite BPs. Reproduced from ref. 15, copyright 2014, with permission from Elsevier.

The dependence of surface conductivity on the preferred orientation of TiN coating, deposited on the Ti bipolar plate by direct current (DC) RMS, was investigated by Yan *et al.*[48] The preferred orientation of TiN film can be set by the N_2 flow rate or the Ti substrate temperature during TiN deposition. Low N_2 flow rate and low substrate temperature help the growth of TiN films along the TiN (111) orientation, showing a much lower ICR than the (200)-oriented coating. A remarkably low ICR value of 1.9 mΩ cm^2 at 140 N cm^{-2} and an I_{corr} of 0.91 μA cm^{-2} under simulated PEMFC conditions were obtained at the N_2 flow of 4 sccm and RT. MIP is a type of PVD based on multiple arc sources. Multiple arc sources ionize the target material, which is accelerated towards the substrate to form a coating. A low-temperature (250 °C) MIP process was utilized to coat a Ti substrate with TiN.[49,50] Low corrosion current density and low ICR were observed for TiN film deposited by MIP on titanium BPs. Li *et al.*[50] evaluated the effect of bias voltage on corrosion resistance and surface conductivity of TiN thin coatings deposited on Ti by MIP. The best results were obtained at a bias voltage of −100 V, with the lowest surface roughness and high compactness. An I_{corr} of 0.47 μA cm^{-2} and an ICR of 3.0 mΩ cm^2 at 140 N cm^{-2} were achieved. Recently, a novel PVD technique, named high-

power impulse magnetron sputtering (HiPIMS), combining the advantages of MIP and RMS, has gained noticeable attention. By utilizing this technique, a high plasma density and high ionization of the sputtered species can be obtained. HiPIMS presents many advantages, such as high film density, good adhesion and smooth surface, making it suitable for obtaining hard coatings. Wang *et al.*[51] coated titanium with a TiN layer by using the HiPIMS technique. They observed that the N_2 flow rate affects the surface characteristics of the coating. The optimized TiN coating under 8 sccm N_2 showed excellent corrosion resistance and electric conductivity. Bi *et al.*[52] coated titanium BPs by a modified powder immersion reaction-assisted coating (PIRAC) method based on the reaction between the Ti substrate and active nitrogen atoms to form a coating. The highest content of TiN and TiN_xO_y was obtained at 1000 °C. As in the case of PN, however, a drawback of this technique is the high nitridation temperature (900–1000 °C).

Multilayer coatings are formed by n ($n \geq 1$) repetitions of two layers, commonly metallic/ceramic and ceramic/ceramic layers. Metal/nitride and nitride/nitride multi-layer (n = 1) coatings were mostly used for PEMFC BPs. Multilayer PVD coatings show enhanced corrosion resistance compared to single-layer coatings due to a lower number of defects and pinholes.[53] Li *et al.* evaluated the effectiveness of Ti/TiN/TaN multilayer coatings either by varying the thickness[54] or by Ti doping of the TaN outer layer.[55] The Ti/TiN/TaN coating was prepared using radiofrequency (RF) and DC RMS at various N_2 ratios. The coating preparation was conducted at a temperature of 300 °C using a MS system that employed a high-purity Ti target as the RF target and a high-purity Ta target as the DC target. A RF Ti target with a power of 200 W was utilized to prepare in an Ar atmosphere the Ti bonding layer, ensuring adhesion between the coating and the substrate. Then, the Ti target power was reduced to 150 W, and N_2 was introduced to form the TiN transition layer. After TiN layer deposition, the RF Ti target was turned off without changing the N_2 ratio, and the DC Ta target was turned on to deposit the TaN layer at a current of 0.3 A. The TiN transition layer and TaN outer layer were deposited in a mixed atmosphere of Ar and N_2. The flowchart of coating preparation is shown in Fig. 6. The N_2 ratio significantly affects the microstructure and phase composition of the

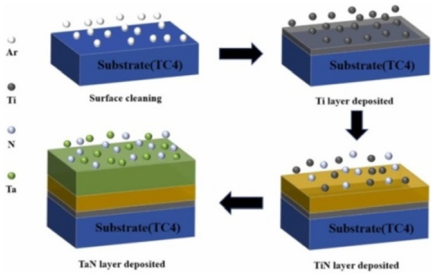

Fig. 6 Flow chart of coating preparation. Reproduced from ref. 54, copyright 2025, with permission from Elsevier.

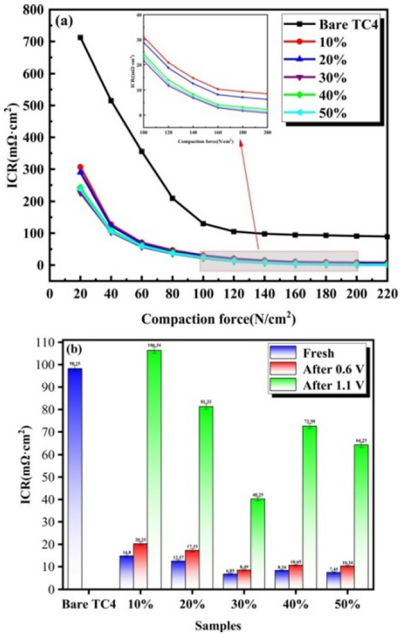

Fig. 7 (a) ICR of uncoated and coated TC4 samples under different compact forces. (b) ICR of the different samples before and after constant potential polarization. Reproduced from ref. 54, copyright 2025, with permission from Elsevier.

coating. The thickness of the TiN layer increases but that of the TaN layer decreases with increasing N_2 ratio, resulting in an improved nitride content in the coating. At an optimal N_2 ratio of 30%, the columnar crystal structure is reduced, leading to improved coating compactness. The Ti/TiN/TaN-30% coating showed very low values of both I_{corr} (0.0654 μA cm^{-2}) and ICR (6.85 mΩ cm^2) (Fig. 7a) and high hydrophobicity (95.5°), meeting the 2025 US DOE standards. As can be seen in Fig. 7b, the ICR of all coated TC4 showed very small changes after polarization at 0.6 V *vs.* SCE. However, the ICR of the coated TC4 remarkably increased following polarization at a higher potential (1.1 V *vs.* SCE) due to intense corrosion of the coating.

By adding a third element, such as Cr, Zr and Nb, to TiN, its corrosion resistance can be enhanced.[53] Li *et al.*[56] fabricated double-layer TiCr/TiCrN coatings for Ti bipolar plates using the MIP technique. TiCr transition layers favor the formation of dense TiCrN surface layers, showing both low I_{corr} (0.099–0.154 μA cm^{-2}) and low ICR (1.3–3.2 mΩ cm^2) under simulated PEMFC conditions. The optimized $Ti_{0.24}Cr_{0.76}/Ti_{0.26}Cr_{0.74}N$ coating demonstrated high stability during ADT under simulated PEMFC conditions. An I_{corr} of 0.25 μA cm^{-2} and an ICR of 6.5 mΩ cm^2 were observed after 100 h of ADT, much lower than the I_{corr} (1.35 μA cm^{-2}) and the ICR (13.5 mΩ cm^2) for single-layer TiCrN after 70 h corrosion test. Then, they varied the sputtering time of TiCr deposition from 30 s to 8 min.[57] At the sputtering time of 1 min, a full lattice matching with TiCrN was obtained. As a consequence, the TiCr/TiCrN coating showed both low I_{corr} (0.070 μA cm^{-2}) and low ICR (2.3 mΩ cm^2). Li *et al.*[58] coated a TC4 substrate with a Ti/TiN/TaTiN multilayer, formed by a

Ti bonding layer, a TiN transition layer, and a Ti-doped (Ta, Ti)N top layer, by MS. The microstructure and phase composition of TaTiN depend on Ti target power. At the optimal Ti target power, the coated TC4 showed the lowest I_{corr} (0.0898 μA cm^{-2}), an ICR value of 6.14 mΩ cm^2, and the highest water contact angle (105.4°), indicating an outstanding hydrophobicity.

TiN-containing composites were evaluated as BP coatings for PEMFCs. Gao *et al.*[59] prepared a C/PTFE/TiN composite coating by a two-step hydrothermal and impregnation process. This composite coating film showed an I_{corr} of 0.009 μA cm^{-2}, an ICR of 13 mΩ cm^2 and a contact angle of 115.53° in simulated PEMFC conditions. While the I_{corr} meets the DOE 2025 requirement, the ICR value exceeds the DOE 2025 target. By replacing the carbon with Ni–P,[60] both the ICR (6 mΩ cm^2) and I_{corr} (0.48 μA cm^{-2}) of the Ni–P/TiN/PTFE composite coating, prepared by electroless plating method (EPM), met the DOE 2025 standards.

2.2.2. Other ceramic coatings. Beyond TiN, many ceramic compounds, such as transition metal nitrides (TMNs),[61–64] transition metal carbides (TMCs),[43,65,66] TaCN,[67] graphene-doped ITO[68] and Ti_3Al/TiAl,[69] were tested as coatings for titanium BPs using different coating techniques. Generally, these coating showed high corrosion resistance and low ICR. Yin *et al.*[61] prepared CrN coating with different thicknesses by MIP. The CrN coatings were formed by Cr and CrN phases, with the Cr/CrN ratio and grain size increasing with the increase of the coating thickness. The CrN coating with a thickness of *ca.* 1.0 μm showed the lowest I_{corr} at 0.6 V (0.594 μA cm^{-2}) and ICR (6.54 mΩ cm^2 at 1.4 MPa) after the corrosion test. Both I_{corr} and ICR decreased with increasing of the coating thickness, ascribed to the increased area fraction of the droplets formed on the coating surface. Chen *et al.*[62] deposited CrN films on Ti BPs by the HiPIMS method. The coating was formed by Cr, CrN and overall Cr_2N phases. The overall HiPIMS pulse length was 800 μs (Fig. 8a). The preparation flow chart is shown in Fig. 8b. Due to the high energy by HiPIMS, the plasma presented a higher ionization rate with high-energy ions, suppressing the growth of columnar structure. The space net structure of amorphous wrapped Cr_2N nanoclusters hindered the corrosion solution from invading the Ti substrate. Moreover, compared to CrN, the higher metallicity of Cr_2N resulted in a higher conductivity of CrN coating by HiPIMS (0.086 μA cm^{-2}) than that of CrN coating by MIP.

Double-glow plasma surface alloying (DGPSA) gained growing interest in recent years. DGPSA is a plasma surface method used to deposit various alloy coatings with outstanding bonding strength and hardness.[70] Glow discharge takes place at both cathode and source electrodes in an Ar plasma atmosphere, in which two power sources are connected, that is, the so-called double-glow discharge: one glow discharge heats an object to attain the alloying temperature, and the second glow discharge bombards the targets to sputter the alloying elements. Under the electric field force, these elements will travel to and diffuse into the surface of the workpiece to form the alloying surface. NbN_x,[63] TiC,[43] TiC-CrC[64] and TaCN[67] coatings were formed by DGPSA on Ti substrates and presented high corrosion resistance, low ICR and good hydrophobicity. Gou *et al.*[66] coated a Ti substrate with a Nb–Cr–C film by an arc ion plating (AIP) method. Most of the Cr was in the element form, while most of the Nb was in the form of NbC. The corrosion current density of Nb–Cr–C obtained by potentiostatic measurements was 0.022 μA cm^2 under simulated PEMFC cathode conditions, while the ICR was 1.15 mΩ cm^2. As shown in Fig. 9, the PEMFC with Nb–Cr–C-coated Ti BPs delivered a MPD of 1160 mW cm^{-2}, close to that of graphite BPs and better than that of bare titanium BPs. The higher contact angle (CA) of Nb–Cr–C-coated titanium indicates a higher hydrophobicity, resulting in more easy water removal.

2.2.3. Carbon-based coatings. Due to their outstanding electrical conductivity and chemical stability, amorphous carbon (a-C) films were utilized as the coating for metal BPs. They are formed by carbon atoms bonded by two hybridization bonds (C_{sp2} and C_{sp3}). The presence of C_{sp2} allows electrons to pass through the film, increasing its electrical conductivity. On the other hand, the presence of C_{sp3}, due to their high bonding energy, makes the film dense and structurally strong. Li *et al.*[71] coated SS316L and TA2 substrates with a-C films, prepared using DC balanced MS. The effect of the type of substrate on the corrosion resistance and ICR was evaluated. The coating showed an outstanding corrosion resistance at 0.6 V *vs.* SCE for

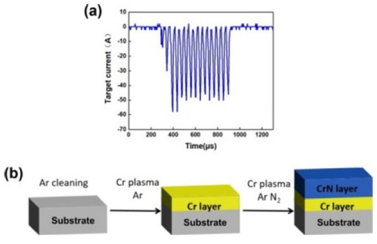

Fig. 8 The current characteristics (a) of HiPIMS pulse shape during CrN deposition and (b) preparation flow chart. From Chen, reproduced from ref. 62, copyright 2022, with permission from Elsevier.

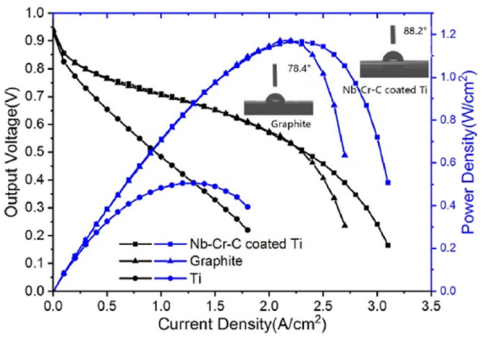

Fig. 9 Performance of single cells with bare titanium, graphite, Nb–Cr–C-coated titanium BPs. Inset: water contact angle with graphite and Nb–Cr–C-coated titanium BPs. Reproduced from ref. 66, copyright 2022, with permission from Elsevier.

both substrates, with the I_{corr} of a-C-coated TA2 lower than that of a-C-coated SS416L. However, at 1.4 V *vs.* SCE, the coating on SS316L presented severe local corrosion, whereas the coating on TA2 did not present any local corrosion, indicating that at high potentials the corrosion resistance of the substrate plays a decisive role. The uncoated SS316L and TA2 showed high ICR, that is, 106.12 and 69.90 mΩ cm^2, respectively. After coating with the carbon film, the ICR decreased to 5.64 and 6.52 mΩ cm^2, respectively. Meng *et al.*[72] coated the surface of titanium foil with a-C film by using the unbalanced magnetron sputtering technique. The I_{corr} of the coating was one order of magnitude lower than that of the substrate, and the ICR value was 10 mΩ cm^2 at 1.4 MPa. Following a long-term potentiostastic polarization test, the ICR of the bare TA1 increased more than three times. Conversely, the ICR of the coated sample only increased by 1.7 mΩ cm^2. Yu *et al.*[73] deposited a-C films on a Ti substrate by AIP at a deposition rate exceeding 100 nm min^{-1} and at various bias voltages (0–70 V). The number of C_{sp2} atoms increased with increasing bias voltage. At the optimal bias voltage (50 V), the a-C coating showed the lowest ICR (1.125 mΩ cm^2) and the lowest I_{corr} (0.00237 μA cm^{-2}) values following long-term potentiostatic polarization under simulated PEMFC conditions. Moreover, the a-C coating formed at 50 V increased the CA of the bipolar plate from 51° to 80°, enhancing water removal. The utilization of a-C as BP coatings, however, presents two drawbacks, that is, a weak coating–substrate bonding and coating detachment, owing to internal stress, and permeation of corrosive media, related to the presence of pinholes, leading to substrate degradation. Effective methods to solve these problems are element doping and the use of multilayer structures. Element doping can reduce internal stress in a-C coatings, and multilayer structures enhance the coating adhesion to the substrate, avoiding the a-C/substrate contact. Wang *et al.*[74] utilized a N/Ti co-doped a-C pseudo-multilayer to coat Ti bipolar plates using the HiPIMS method in the presence of N_2. For comparison, an a-C:Ti coating was also deposited on the Ti substrate by HiPIMS without an N_2 atmosphere. The excellent periodicity of Ti and C elements in the a-C:Ti coating and Ti, N and C in the a-C:N–Ti coating suggested the formation of a multilayer structure, but a layered structure was not confirmed by TEM images. The presence of N gave rise to the transition from sp^2 to sp^3 hybridization state in a-C and the conversion of Ti–C to Ti–N bonds, enhancing the corrosion resistance but increasing the interfacial resistance. As a consequence, as shown in Fig. 10, going from an a-C:Ti to an a-C:N–Ti coating, the I_{corr} decreased from 2.89 μA cm^{-2} to 0.876 μA cm^{-2}, and the ICR increased from 4.15 mΩ cm^2 to 6.69 mΩ cm^2. Yan *et al.*[75] deposited a multilayer coating consisting of an a-C:H–TiC composite outer layer, a TiCN interlayer, and a TiN inner layer on a Ti substrate by HiPIMS. The high compatibility of TiN with Ti facilitates the adhesion of the coating to the titanium substrate. The a-C:H/TiC composite layer was obtained by sputtering the Ti target with C_2H_2 at 30 sccm, 40 sccm, 50 sccm and 60 sccm. The number of sp^2 bond atoms increased with increasing C_2H_2 flow rate, leading to a decrease of the I_{corr} but an enhancement of the ICR. The I_{corr} of the film prepared at a C_2H_2 flow rate of 60 sccm in simulated PEMFC conditions was 0.66 μA cm^{-2}, and the ICR at 1.4 MPa was 1.6 mΩ cm^2. In a similar way, Luo *et al.*[76] coated a Ti substrate with a multilayer layer structure formed by a-C as the outer layer, TiC as the interlayer and Ti as the inner layer. The coated Ti BP showed an I_{corr} of 0.88 μA cm^{-2} under simulated PEMFC conditions, a water CA of 97.9° and an ICR value of 1.66 mΩ cm^2 at 1.4 MPa. Gou *et al.*[77] coated TA1 with NbC/a-C:H films with various Nb/C ratios by the AIP method. The film hardness, adhesion strength and the ICR increased with increasing NbC content, whereas the corrosion resistance increased with increasing a-C:H content in the coating. The lowest values of I_{corr} and ICR were 0.09 μA cm^{-2} and 0.77 mΩ cm^2, respectively. Pukha *et al.*[78] deposited a conductive carbon nanocomposite coating (CNC) on a Ti alloy (VT1-0, 99% Ti, 0.25% Fe) by a C_{60} ion beam irradiation technique at various accelerating voltages and substrate temperatures. A CNC is formed by graphite nanocrystals embedded in a diamond-like matrix. The strength and adhesion of this coating were determined by nanoindentation scratch tests: coating delamination and cracking were not found before failure, indicating that the CNC has low internal stress. The critical load of the coefficient of friction was higher than 50 mN, showing good anti-scratching properties and strong adhesion of the coating to the Ti alloy substrate. The lowest I_{corr} (0.001 μA cm^{-2}) and ICR (2.6 mΩ cm^2) values were obtained at 400 °C and an accelerating voltage

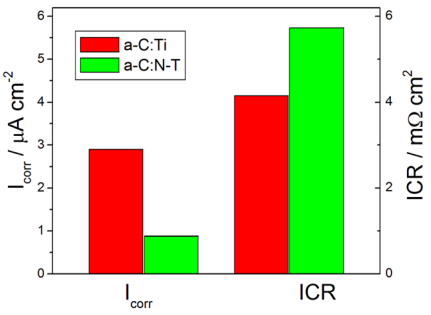

Fig. 10 Histogram of I_{corr} and ICR values of a-C:Ti and a-C:N–Ti from data in ref. 74.

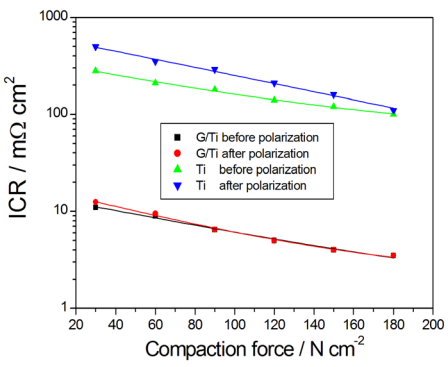

Fig. 11 ICR of unpretreated Ti and G/Ti before and after polarization. Reproduced from ref. 79, copyright 2019, with permission from Elsevier.

of 6 kV and 8 kV, respectively. The high number of sp^3 bonds in the diamond leads to a high CA (*ca.* 96°).

Graphene and reduced graphene oxide were also used as coating for titanium BPs. Wang *et al.*[79] coated Ti sheet with graphene with a thickness of only 50 nm by pulse electrodeposition. By potentiodynamic and potentiostatic tests under simulated PEMFC conditions, the I_{corr} of the graphene-coated Ti sheet was around 0.1 μA cm^{-2}, significantly lower than that of uncoated Ti sheet. In addition, the thin graphene film on the Ti sheet showed a low ICR, meeting the DOE requirements on BPs. Fig. 11 shows the dependence of the ICR of coated and bare Ti on the compaction force. As can be seen in Fig. 11, the ICR of uncoated Ti was much higher than that of graphene-coated Ti. Moreover, the ICR of bare Ti increased significantly following 5 h of potentiostatic polarization. Conversely, the increase of ICR was hardly appreciable after the same polarizations. Liu *et al.*[80] electrophoretically deposited a modified graphene layer on titanium BPs. *p*-Phenylenediamine (PPD) was first grafted onto graphene oxide (GO) to obtain modified graphene oxide (MGO); then, MGO was electrophoretically deposited on titanium BPs, followed by reduction of MGO, obtaining reduced MGO (RMGO@Ti)-coated Ti. Under simulated PEMFC conditions, RMGO@Ti showed a corrosion current of $<10^{-6}$ A cm^{-2} and an ICR of 4 mΩ cm^2 at 1.4 MPa, both considerably lower than those of bare Ti. Yu *et al.*[81] coated TC4 BPs with directly grown vertical graphene (VG) by the plasma-enhanced chemical vapor deposition (PECVD) method. Under simulated PEMFC conditions, the I_{corr} and the ICR of VG-coated TC4 were remarkably lower (0.043 *vs.* 0.523 μA cm^{-2} and 1.48 *vs.* 150 mΩ cm^2), respectively, and the water CA was considerably higher (142.2° *vs.* 74.1°) than that of the uncoated one.

To avoid the drawback related to the use of conventional carbon deposition techniques, recently a roll-to-roll doctor blade coating method was proposed.[82] The doctor blade process can be utilized to create a coating by putting a slurry formed by a suitable material, a solvent, and a binder onto a substrate, then by drying and sintering. Hwang and Kim[82] used this technique to coat carbon onto a TiO_2 surface. First, TiO_2 was deposited onto the Ti surface, followed by the coating of TiO_2 with carbon using the doctor blade technique. The corrosion resistance and BP/GDL contact resistance were evaluated before and after ADT under simulated PEMFC conditions. As can be seen in Fig. 12, before ADT, the I_{corr} of the coated Ti considerably decreased compared to that of the uncoated substrate. After ADT, the I_{corr} of the bare Ti decreased from 0.49 μA cm^{-2} to 0.025 μA cm^{-2}, while that of the coated Ti increased from 0.048 μA cm^{-2} to 0.408 μA cm^{-2}. For uncoated Ti, the decrease of I_{corr} after ADT was due to the formation of a passivation layer, leading to a reduced corrosion rate. In the case of coated Ti, the TiO_2 layer in part dissolved during ADT, decreasing corrosion resistance. Conversely, the ICR of the coated Ti was remarkably lower than that of the uncoated one both before and after ADT. These results indicate that the doctor blade method can be a practicable alternative to the commonly used processes to form Ti BP coatings.

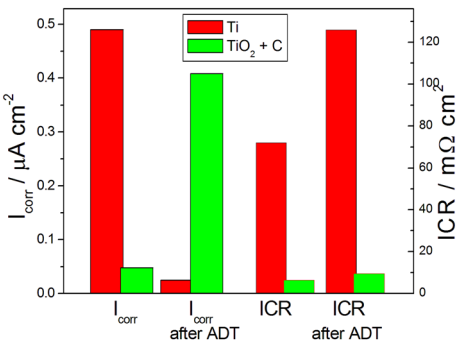

Fig. 12 Histogram of I_{corr} and ICR values of TiO_2 + C-coated Ti and bare Ti before and after ADT from data in ref. 82.

Literature data on I_{corr}, obtained by potentiodynamic polarization measurements and ICR of some coatings for titanium bipolar plates are reported in Table 2. An effective coating has to have a high corrosion resistance and a low contact resistance between BP and GDL. The lower the values of I_{corr} and ICR, the better the characteristics of a coating material.

Both the values of I_{corr} and ICR of uncoated Ti fall in a wide range (I_{corr} from 0.5 to 500 μA cm^{-2}, with most between 1 and 50 μA cm^{-2}, and ICR from 15 to170 mΩ cm^2, from the references reported in Table 2), depending on the purity grade of Ti and the BP fabrication method. All these values, with only a few exceptions for I_{corr}, do not meet the US DOE 2025 targets. Conversely, most of the I_{corr} and ICR values of coated Ti meet the DOE 2025 targets. Most of the values of the $A_{corr}^{Ti/C}$-to-A_{corr}^{Ti} (A = I_{corr} or ICR) ratio, where $A_{corr}^{Ti/C}$ and A_{corr}^{Ti} are the A values of coated and uncoated Ti from literature data in the references reported in Table 2, fall in the 0.01–0.1 range. This result indicates that after coating, most of both I_{corr} and ICR values are more than 1 order of magnitude lower than that of the uncoated one. Generally, there is no correlation between the values of I_{corr} and ICR and the manufacturing method. For TiN, the lowest I_{corr} was obtained by PN. Very low I_{corr} values were obtained by using multilayer coatings. The lowest ICR values were obtained by AIP and MIP. To evaluate the durability, potentiostatic polarization measurements were also carried out at the potential of 0.6 V. Generally, for both doped and undoped Ti, the curve of current density *vs.* time initially decreases due to the formation of a passivation layer; then, when the formation of the passivation layer is complete, it reaches a steady state. After the potentiostatic polarization test, the ICR value of doped and undoped Ti was higher than that before the test due to enhanced surface roughness and higher insulating properties of the passive film. Thus, after the potentiostatic polarization test the I_{corr} continues to meet the DOE 2025 requirements, while the ICR value may no longer meet the DOE 2025 target, as in the case of the TaCN (11.3 mΩ cm^2),[67] a-C (11.7 mΩ cm^2)[72] and Ti_3Al/TiAl (17.8 mΩ cm^2)[69] coatings.

Table 2 Literature data on I_{corr} and ICR of some coatings for Ti bipolar plates. Titanium: I_{corr} = 0.5–500 μA cm^{-2}; ICR = 15–170 mΩ cm^2. Bold data: >DOE 2025 targets

Coating, coating technique	Substrate	I_{corr}/μA cm^{-2} US DOE 2025 target: <1 μA cm^{-2}	ICR/mΩ cm^2 (140/150 N cm^{-2}) US DOE 2025 target: ≤10 mΩ cm^2	Reference
TiN, PN/900 °C	Ti	**89.80**	**38.58**	44
TiN, PN	TA2	0.195 (30 min nitriding)	1.99	45
TiN, PN/700 °C	TA1	0.016 (4 h nitriding)	4.94	46
TiN, liquid phase PN	TC4	0.57	6.0	47
TiN(111), RMS	Ti	0.91	1.9	48
TiN, MIP	Ti	0.47	3.0	50
TiN, HiPIMS	Ti	0.278	3.51	51
TiN, PIRAC nitriding	TC4	0.009	4.6	52
TiN/TaN-30%, RMS	TC4	0.0654	6.85	54
TiCr/TiCrN, MIP	Ti	0.099–0.154	1.3–3.2	56
TiCr/TiCrN, MIP	Ti	0.070	2.3	57
Ti/TiN/TaTiN	TC4	0.0898	6.14	58
C/TiN/PTFE, Hydrotherlmal impregnation	TA2	0.009	**13**	59
Ni–P/TiN7PTFE, EPM	TA2	0.48	6	60
CrN MIP	TA2	0.015	6.54	61
Cr_2N, HiPIMS	Ti	0.086 (N_2 flow ratio 2 sccm)	6.14 (N_2 flow ratio 2 sccm)	62
NbN_x, DGPSA	TC4	**8.92**	7.29	63
NbN, RMS	Ti	0.23 (N_2 flow ratio 3 sccm)	5	64
TiC, DGPSA	TA1	0.137	7.6	43
TiC-CrC, DGPSA	CP-Ti grade 2	0.50	0.87	65
Cr-NbC, AIP	TA1	—	1.15	66
TaCN, DGPSA	T40	0.08	9.6	67
G-ITO, dip coating	TA2	0.06	—	68
Ti_3Al/TiAl, heat treatment with Al_2O_3	TC4	0.076	4.9	69
a-C, DCBMS	TA2	0.051	6.52	71
a-C, MS	TA1	0.79	10.0	72
a-C, AIP 50 V bias voltage	TA1	0.065	1.13	73
a-C:Ti, HiPIMS	Ti	**2.89**	4.15	74
a-C:N–Ti, HiPIMS	Ti	0.876	6.69	
a-C:TiC/TiCN/TiN HiPIMS 60sccm	Ti	0.66	1.6	75
a-C/TiC/Ti, MIP	TA1	0.88	1.66	76
a-C:H/NbC, AIP	TA1	0.09	0.77	77
CNC, C_{60} ion beam	VT1-0	0.007	2.6	78
G, PE	Ti	0.25	4.0	79
RMGO, ED	Ti	0.755	4.0	80
VG, PECVD	TC4	0.034	1.48	81
TiO_2 + C, doctor blade	Ti	0.048	6.0	82

Summarizing, the most suitable coating for Ti bipolar plates is TiN due to excellent corrosion resistance, high conductivity, high adhesion strength to Ti, thermal expansion coefficient close to that of Ti, wide industrial feasibility, low cost, and extensive research as well. A weak coating–substrate bonding and coating detachment, instead, are drawbacks regarding the use of a-C as BP coating. Thus, a-C cannot be used alone as it is but requires element doping or the use of multilayer structures.

Regarding the deposition methods, conventional consolidated deposition techniques, including PVD, CVD and PVD/CVD-derived technique such as RMS, MIP and HiPIMS, have proven to be effective for improving the corrosion resistance and electrical conductivity of Ti bipolar plates, but they require high-vacuum conditions, precise gas mixing, and strict temperature control. Such requirements are a significant challenge for large-scale production of PEMFC BPs, including increased equipment costs, maintenance burden, and limited scalability. To overcome these limitations, a roll-to-roll doctor blade coating method was proposed. This technique enables environmentally friendly coatings without the need for vacuum or gas-phase control while offering superior process efficiency and cost-effectiveness.

2.3. Microstructural modification of the titanium surface

The substrate material can affect the corrosion resistance of the coating. For example, using the same deposition method, TiN-coated SS410 showed a higher I_{corr} under simulated anode conditions than TiN-coated SS316L due to the lower corrosion resistance of SS410 than that of SS316L.[83] In the same way, the corrosion current density of a-C-coated titanium (TA2) was lower (0.051 μA cm^{-2}) than that of a-C-coated SS316L (0.148 μA cm^{-2}) due to the higher I_{corr} of SS316L than that of TA2.[71] Thus, the improvement of the corrosion resistance of the substrate by using surface modification technologies is necessary to enhance the overall corrosion resistance of the BPs. The grain size, grain

boundary type, and texture intensity influence the corrosion resistance of materials. The microstructure of titanium was modified by using different methods. Equal channel angular pressing (ECAP) is a method to obtain ultrafine grains in materials. Balyanov *et al.*[84] evaluated the corrosion resistance in acid solutions of Ti with both ultrafine-grained (UFG, grain size 10–1000 nm) microstructure obtained by ECAP and coarse-grained (CG) microstructure, formed by annealing at 800 °C, resulting in a grain size of 7 μm. The UFG Ti showed higher corrosion resistance than CG Ti due to fast passivation of UFG Ti and the impurity segregation to grain boundaries in CG Ti. Differential speed rolling (DSR) is a widely utilized method to modify the grain and texture characteristics of a material. Bare Ti sheets with UFG microstructures were obtained by high-ratio differential speed rolling (HRDSR) at different roll speed ratios and roll temperatures.[85] The HRSDR-processed Ti sheets at a higher speed ratio or a lower temperature showed a smaller grain size and higher strength. The UFG Ti showed high corrosion resistance in acid solutions. The Ti grain refinement by HRDSR enhances the corrosion resistance by modifying the growth kinetics of the passivating film. The Ti with the smallest grain size, that is, HRDSR processed at room temperature, presented the lowest I_{corr}. Liu *et al.*[86] used cold DSR at various roller speed ratios (RSRs) to enhance the corrosion resistance of pure Ti. The Ti sheet obtained at an RSR of 2, having the highest mechanical strength and corrosion resistance (I_{corr} 0.43 μA cm^{-2}), was used for rubber pad forming Ti BPs. The I_{corr} of pure Ti at the operating temperature of PEMFC (75 °C) was 1.27 μA cm^{-2}. Krállics *et al.*[87] processed Grade 2 Ti by warm caliber rolling, obtaining an UFG microstructure with high tensile strength and good ductility at room temperature. The ball-burnishing (BB) process is a cold surface plastic deformation method based on moving and compressing a hard ball on the surface of materials. Shliakhetka *et al.*[88] studied the corrosion resistance of highly porous Ti in acid solution by BB. BB made easier the healing of pores within the deformed surface layer, reducing the porosity from 16.4% to 1%. Following BB, I_{corr} decreased from 3.74 to 1.52 μA cm^{-2}, ascribed to the reduction in the surface area in contact with a harsh environment and the formation of a passivating film. Kim and Kim[89] investigated the effect of annealing on the corrosion resistance in acid solution of the UFG Ti obtained by HRDSR. Post-rolling annealing decreased the corrosion resistance of UFG Ti, reducing dislocation density and residual stress and maintaining an UFG and a strong texture. Zhu *et al.*[90] evaluated the influence of the annealing time (from 5 to 60 min) at 650 °C on the microstructure and corrosion resistance of cold-rolled Ti–Nb–Ni sheets. In non-annealed cold-rolled Ti–Nb–Ni, tips of precipitated Ti_2Ni were formed, resulting from sheet deformation. In annealed Ti–Nb–Ni, notwithstanding the increase of grain size, the blunt Ti_2Ni tips led to an increase of the corrosion resistance. I_{corr} decreased with increasing annealing time from 0.40 μA cm^{-2} for non-annealed Ti alloy to 0.13 μA cm^{-2} for 60 min annealed Ti-Nb-Ni in a simulated PEMFC solution.

2.4. Titanium alloys as BP substrates

Although coating improves the corrosion resistance and ICR of Ti substrates, they are, however, critical factors due to the presence of defects, including pinholes, on coating during preparation. Taking into account the corrosion resistance, conductivity and formability, coated titanium cannot fully satisfy the requirements for its use as BPs in PEMFC. Moreover, during PEMFC operation, fluoride ions released from Nafion® membranes can dissolve the protective TiO_2 film, thereby leading to a decrease of Ti corrosion resistance.[91] A way to alleviate these drawbacks is the use of uncoated titanium alloys as BP substrates.

2.4.1. Microalloyed and low-alloyed titanium. Taking into account the formability and costing, the number of alloying elements has to be in a relatively low level. Microalloying and low-alloying are widespread approaches to improve the corrosion resistance and the ICR of titanium through utilization of limited but specific alloys. Microalloyed titanium is a type of titanium alloy that contains small amounts of alloying elements (<1%), including Nb, V, Ni and Mo. Low-alloy Ti materials (Ti >80%) possess the same outstanding properties as pure titanium together with enhanced corrosion resistance and ICR. To improve the ICR of the oxide layer different microalloyed and low-alloyed titanium alloys, forming conductive and passivating oxides, were investigated for their use as PEMFC bipolar plate substrates. Aukland *et al.*[92] developed alloys that form conductive and chemically stable oxides in a PEMFC environment. Five alloys of Ti with Ta or Nb were evaluated. Nb can enhance the electrical conductivity of Ti BPs *via* electron hopping mechanism. The oxides of all alloys showed lower ICR than bare Ti oxide. The oxide films on Ti–Nb and Ti–Ta surface alloys remained conductive and chemically stable in more concentrated solutions than that under PEMFC conditions. Ti alloys having 3% Ta or Nb were the most suitable for use as BP materials. One element which increases Ti corrosion resistance is Ni, possessing similar effects to Pt group metals to shift the corrosion potential towards passive Ti regions.[93] Zhu *et al.*[94] fabricated a Ti–Nb–Ni foil by a cold-rolling process for its use as a BP substrate. The ICR values of the Ti–Nb–Ni foil at 1.4 MPa satisfied the DOE 2025 target and were lower than those of some bare SSs. The suitable ICR values were ascribed to the improved conductivity of the oxide film formed on the Ti–Nb–Ni by the presence of Nb. Song *et al.*[95] investigated the corrosion resistance and the ICR of Ti–Ta alloys in the Ti-7Ta, Ti-8.3Ta and Ti-9.6Ta compositions, and Ti–Al–Ta alloys in the Ti-2.6Al-5.8Ta, Ti-3.8Al-8.6Ta and Ti-5Al-11.3Ta compositions. The cathodic corrosion current density of all these alloys was lower than that of the reference TC4 (Ti-6Al-4 V) alloy in the PEMFC simulated cathodic environment (0.5 mol L^{-1} H_2SO_4 + 2 × 10^{-6} HF) at 0.6 V *vs.* SCE. Among them, the Ti-8.3Ta

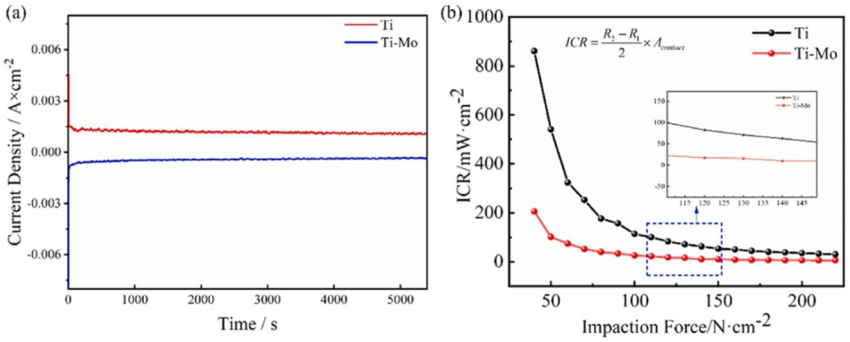

Fig. 13 (a) Potentiodynamic polarization curves of Ti and Ti-0.35Mo. (b) ICR values after potentiostatic polarization for Ti and Ti-0.35Mo alloy. Reproduced from ref. 96, copyright 2024, with permission from Elsevier.

alloy showed the smallest I_{corr} (0.72 μA cm^{-2}). The ICR value at 1.5 MPa decreased with increasing Ta content and was lower than that of bare Ti and TC4. The ICR of Ti-5Al-11.3Ta alloy was the smallest (18.3 mΩ cm^{-2}) and the I_{corr} was 0.91 μA cm^{-2}. Yuan *et al.*[96] prepared a Ti-0.35Mo alloy and evaluated the I_{corr} and ICR values. Ti-0.35Mo showed an I_{corr} *ca.* two orders of magnitude lower than that of pure Ti. Constant anode potential polarization measurements were performed at −0.1 V *vs.* SCE. As shown in Fig. 13a, in a simulated PEMFC anodic environment, the polarization curve for Ti showed a positive trend (I_{corr} *ca.* 1.4 10^{-3} A cm^{-2}). Conversely, the polarization curve for Ti-0.35Mo showed a negative trend (I_{corr} *ca.* −6.2 10^{-4} A cm^{-2}), attesting that Ti-0.35Mo is more corrosion resistant than Ti. The ICR decreases with increasing pressure (Fig. 13b). At 140 N cm^{-2}, the ICR value for Ti-0.35Mo in the simulated PEMFC cathodic environment was 9.80 mΩ cm^2, slightly lower than the DOE 2025 target.

Fluoride ions can seriously deteriorate the corrosion resistance of titanium: fluoride ions can react with the protective oxide film on titanium, resulting in the dissolution of the protective film.[97] The reaction between TiO_2 and F^- is as follows:[97]

$$TiO_2 + 4H^+ + 6F^- \rightarrow TiF_6^{2-} + 2H_2O \quad (1)$$

As a consequence, the formation of unpassivated titanium regions decreases the corrosion resistance of the bipolar plate. Wang *et al.*[98] observed that there is a threshold value of the F^- concentration for Ti corrosion in 0.05 M H_2SO_4 solutions, between 0.0005 M and 0.002 M. When the F^- concentration was higher than the threshold value, multiple corrosion potentials were found in potentiodynamic polarization curves. F^- can change the structure of the film formed on titanium at open circuit voltage (OCV) from a dense to a porous barrier. Alloying can be a valid method to enhance Ti corrosion resistance in F^--containing acidic solutions. Nakagawa *et al.*[99] investigated the effect of F^- concentration and pH on the corrosion resistance of bare Ti and Ti-6Al-4 V, Ti-6Al-7Nb and Ti-0.2Pd alloys. Bare Ti, Ti-6Al-4 V and Ti-6Al-7Nb alloys showed low corrosion resistance even in a low F^- concentration in acid solution. The Ti-0.2Pd alloy showed high corrosion resistance than bare Ti, Ti-6Al-4 V and Ti-6Al-7Nb alloys in a wide range of pH and F^- concentrations due to the presence of Pd on the surface, favoring a repassivation of Ti. TA12 (chemical composition Ti-0.3Mo-0.8Ni), belonging to a near-alpha titanium alloy, was developed in the United States in the 20th century to aim to replace the high-cost Ti-0.2Pd alloy. Wang *et al.*[91] evaluated the dependence of I_{corr} on the F^- concentration for pure Ti and Ti-0.2Pd and Ti-0.3Mo-0.8Ni alloys. The I_{corr} of all three material samples increased with F^- content. The I_{corr} of bare pure Ti was the same as that of Ti alloys for a F^- content lower than the threshold value of bare Ti. For F^- content >0.001 M (threshold value of bare Ti), the I_{corr} values of Ti-0.2Pd and Ti-0.3Mo-0.8Ni were much lower than that of bare Ti, ascribed to the spontaneous passive behavior of these alloys with respect to the active behavior of pure Ti. By theoretical calculations it was demonstrated that the presence of Mo and Ni in the TA12 alloy decreases the hydrogen evolution reaction (HER) overpotential on the Ti surface.[100] The HER overpotential was 0.734 eV for Ti-Mo, 0.569 eV for Ti-Ni, and 0.512 eV for Ti-0.3Mo-0.8Ni. The increase of the HER rate facilitates the formation of an anodic passivation film, remarkably enhancing TA12 alloy corrosion resistance. Ti alloys, however, are still corroded at higher fluoride concentrations. Zhu *et al.*[94] studied the corrosion resistance of Ti–Nb–Ni in 0.5 M H_2SO_4 solution with various F^- content at different temperatures. The corrosion resistance of Ti–Nb–Ni decreased with increasing temperature and fluoride concentration. The threshold F^- content was 100–200 ppm at 20 °C and 50–100 ppm at 40 °C/80 °C.

2.4.2. NiTi (1 : 1) alloy. Recently, Li *et al.*[101] fabricated a melting cast NiTi alloy in the atomic ratio of 51 : 49 in a vacuum arc melting furnace. This NiTi alloy showed a significantly lower ICR value at 1.4 MPa (16.8 mΩ cm^2) compared with pure Ti (88.6 mΩ cm^2) as well as improved corrosion resistance compared with pure Ni. The improved ICR was ascribed to the presence of metallic Ni in the passive film, enhancing charge conduction. Moreover, a higher hardness of the NiTi alloy than that of bare Ti and bare Ni was observed.

3. Gas diffusion layer

The GDL is placed between the CL and the BP on each side of the PEMFC and plays many roles within the fuel cell:[102–104] (1) it provides electrical connection between the CL and the BP; thus it has to have high electronic conductivity; (2) it conducts heat away from the CL; thus it has to have high thermal conductivity; (3) it gives mechanical support to the brittle CL, so it has to have high mechanical stability; (4) it provides transport pathways for reactant gases from the flow channels to the CLs, so the GDL has to have suitable mass transport; (5) it makes easy the removal of excess liquid water; thus it has to have proper wettability. Single-layer GDL consists only of a macroporous substrate (MPS). The commonly utilized GDL in PEMFCs, however, is dual layer, in which the MPS is coated with a microporous layer (MPL). The MPL decreases the contact resistance between the CL and the MPS and improves water management in the membrane electrode assembly, leading to an enhancement of fuel cell performance. Additionally, a hydrophilic layer (HL) can be placed on the MPL to improve the performance in low-humidity conditions.

3.1. Gas diffusion backing (macroporous substrate)

The use of carbon materials as the GDB substrate is due to their high electrical conductivity and the low cost. Despites this, carbon is far from being a fully satisfactory choice for GDB due to its low strength and limited corrosion resistance. Carbon is inclined to corrosion at high potential fuel cell operation.[105] The brittle nature of carbon is not very suitable to molding and processing, making the microstructural control difficult. Thus, research efforts have been addressed to metal materials as the substrate for the GDL due to their high strength. Metallic materials can be divided into machined metal, metal foam and metal fiber. Steel has high strength but limited electrical conductivity and corrosion resistance. Conversely, Ti has high strength, lower density and outstanding corrosion resistance. Hence, porous titanium is more appropriate for utilization as GDB than carbon and steel.[105] The challenge of the use of Ti as GDB, however, is Ti manufacturing with controlled porosity, thickness, and pore morphology. Moreover, the cost of porous Ti is another factor limiting its application. As carbon cannot be used for the oxygen electrode of unitized reversible fuel cells (URFCs), as at the high potential of the oxygen electrode during electrolysis mode carbon material is inclined to corrode, Ti, due to its high conductivity and corrosion resistance even under high potential and acidic environment, is commonly used as the oxygen electrode GDB of a URFC.[106–108] In this work, however, only the use of Ti as GDL substrate in PEMFCs will be considered. Ti sinter,[109] Ti fiber felt,[110,111] and Ti foam[112] were used as Ti GDB in PEMFCs. Different preparation methods such as freeze cast,[112] micromachining[113] and 3D printing[114,115] were utilized to fabricate GDBs. Generally, Ti-based GDLs are in the single-layer form, that is, the GDL coincides with the GDB. First, Hottinen *et al.*[109] investigated the utilization of Ti sinter as GDB in a PEMFC. They observed that the ICR between Ti sinter and MEA was very large. The ICR can be reduced by Pt coating on the Ti sinter surface. Ti sinter on the PEMFC cathode side increased the mass diffusion overpotential likely due to the inadequate water removal. Pt coating reduced this overpotential owing to the improved hydrophobicity. However, the performance of the PEMFC with Pt-coated Ti sinter as GDB was lower than that with carbon paper. Ti sinter can be useful when high current densities are not necessary. Ti sinter cost is not much different from that of carbon paper and cloth. Pt coating increases the sinter cost, but so long as the sinter operates as combined GDB/BP, the convenience of sinters is remarkably enhanced because there is no longer any need for a separate BP. Fushinobu *et al.*[113] proposed a novel ordered porous Ti single-layer GDL fabricated by using the micromachining technique. Ti thin films with 1 to 10 μm thickness were micromachined to obtain columnar vertical micro through-holes in the thickness direction. By using Ti thin films instead of carbon-based materials, the thickness and electrical resistivity were remarkably decreased, suggesting the possibility of high performance GDLs. The feasibility to be used as GDLs in PEMFC was evaluated. Smaller through-hole diameter and thinner Ti thickness than carbon GDL improved the PEMFC performance. Choi *et al.*[112] proposed a freeze-cast Ti foam anode single-layer GDL for PEMFC. The PEMFC with Ti foam GDL showed a current density *ca.* 166% higher than that with a carbon fiber GDL, with and without MPL, due to its unique 3D structure, supporting anodic reactions. Moreover, it showed excellent corrosion resistance with stable thickness and weight in an accelerated corrosion test, while the carbon GDL suffered considerable reductions in the weight and thickness. Jayakumar *et al.*[114] fabricated a Ti-based GDL using a 3D printing technique incorporating selective laser sintering. This technique is more cost-effective than manufacturing a conventional GDL. A 20% Ti/80% polyamide composite powder was spread on the built platform layer upon layer, obtaining a uniform dispersion and a flat top surface. The resulting performance of the MEA with this GDL was far lower than that of the MEA with the carbon-based GDL due to the lower electrical conductivity. Wang *et al.*[115] proposed an integrated flow field-gas diffusion layer (*i*-FF-GDL) fabricated by 3D printing of TiH_2 ink, then decomposed by high-temperature treatment to form a conductive, hydrophilic and porous Ti "bone" structure. A comparison of the common carbon-based PEMFC configuration and the integrated *i*-FF-GDL PEMFC configuration is reported in Fig. 14. They compared the performance of alkaline PEMFCs with *i*-FF-GDL and conventional carbon paper GDL and graphite serpentine FFs. Compared to the cell with conventional GDL and FF, the performance of the PEMFC with *i*-FF-GDL showed a considerable enhancement at high current densities. The MPD of the PEMFC with *i*-FF-GDL was 15% and 8% higher than that of the cell with GDL and FF under H_2/O_2 and H_2/air conditions, respectively. Moydien *et al.*[110] compared Ti fibre felts single-layer GDL and conventional carbon GDLs, both in different

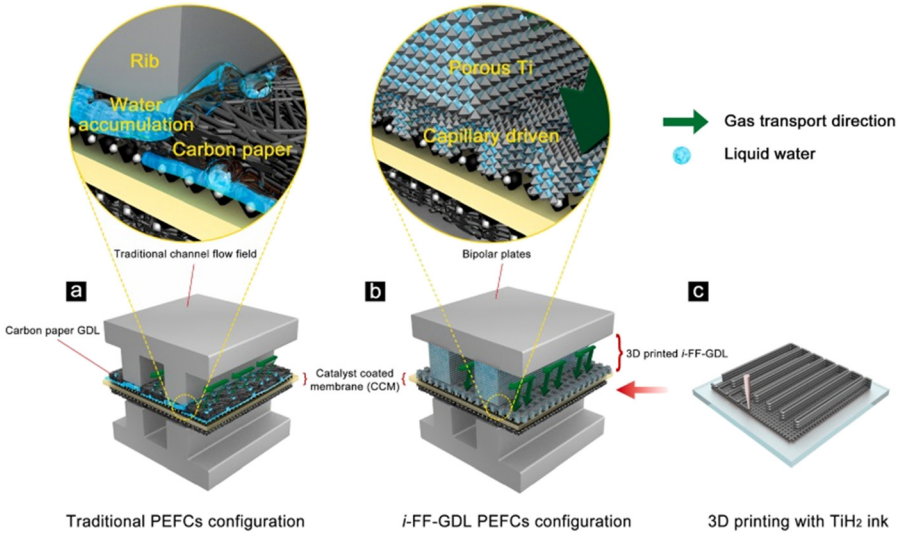

Fig. 14 Schematic diagram of traditional PEMFC configuration (a), *i*-FF-GDL PEMFC configuration (b) and the 3D printing process (c). Reproduced from ref. 115, copyright 2021, with permission from Elsevier.

thicknesses, as cathode GDLs for PEMFCs. The Ti fibre felt was coated with 0.2 μm Pt to avoid Ti oxidation. SEM images of the carbon (C-GDL) and titanium fibre (PTF-GDL) are reported in Fig. 15. It can be observed that the C-GDL fibres are cylindrical while the PTF-GDL fibres have flat edges. In the case of the PTF-GDL fibres, flat edges lay upon each other, while the cylindrical shape of C-GDL fibres results in single-point contact between the C-GDL fibres, leading to a lower contact resistance for PTF-GDLs than for C-GDLs.

For all GDL thicknesses, the polarization curve of PEMFCs with Ti felt GDL delivered an enhanced performance than the cells with conventional GDL. Compared to the cells with C-GDLs, the performance enhancement of the cells with Ti-GDLs begins at medium current densities and increases at high current densities. The difference in the performance of the PEMFCs with different GDLs was ascribed to a difference in the ohmic resistance and mass transport properties. Ma *et al.*[111] investigated the performance of a PEMFC with a Ti felt GDL before and after hydrophobic treatment (carbon plating and application of an acetylene black MPL). The PEMFC with hydrophobic-treated GDL delivered a remarkably better performance compared to the untreated one. The PEMFC with untreated GDL presented a remarkable flooding and a fast voltage drop at high current density. The hydrophobic treatment of the GDL remarkably enhanced water drainage of the PEMFC at high current density. Moreover, the performance at low/medium current density (<1.3 A cm^{-2}) of the Ti GDL fuel cell after hydrophobic treatment was almost the same as that of the conventional C-GDL.

Finally, Kawachino *et al.*[116] developed a carbon-free catalyst-integrated nanostructured electrode with porous Ti support. Porous Ti sheets were etched in NaOH and heat-treated at 400 °C, resulting in TiO_2 nanostructure formation on the Ti fiber surface, followed by Pt deposition onto the fiber surface. The Pt-decorated nanostructured Ti sheets played in a PEMFC at the same time the role of the catalyst, catalyst support, GDL and current collector, overcoming carbon corrosion drawback. The initial performance of the Pt/Ti system was lower than that of a commonly used Pt/C system, but it presented considerable stability following potential cycling.

Summarizing, the best choice to fabricate GDL is the 3D printing technique. This technique is more cost-effective than manufacturing a GDL by using conventional methods. The main interesting part of this section is the use of integrated carbon-free Ti BP/GDL systems, as in the case of Ti sinter, that operates as a combined GDB/BP, Ti "bone" structure (*i*-BP-GDL), fabricated by 3D printing, and Pt-decorated nanostructured Ti sheets, playing the role of catalyst, catalyst support, GDL and current collector, overcoming the carbon corrosion drawback.

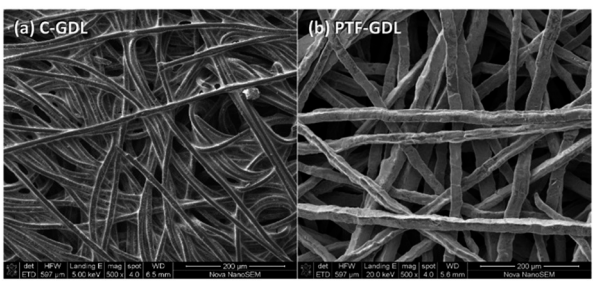

Fig. 15 SEM images of (a) the C-GDL and (b) the PTF-GDL substrates. Reproduced from ref. 110, copyright 2023, with permission from Elsevier.

3.2. Hydrophilic layer

An MPL, commonly formed by carbon black and a polytetrafluoroethylene (PTFE) binder, is generally placed on top of the GDB for water removal from the catalyst layer (CL).[117,118] Moreover, the MPL minimizes the contact

resistance between the CL and the GDL and provides support for the CL, limiting the loss of the catalyst into the GDL.[117] Commonly, the MPL has hydrophobic properties, but enhancing the hydrophilic properties of the MPL can prevent membrane dehydration at the interface with the CL under low-humidity conditions. However, this can also lead to excessive flooding under high-humidity conditions. On the other hand, the enhancement of the hydrophobic properties facilitates the smooth removal of water, offering advantages under high-humidity conditions, but this can accelerate membrane dehydration and hinder proton conductivity under low-humidity conditions. Thus, the wettability of GDLs has trade-offs, as it is optimized for specific humidity conditions. The decrease of PTFE content in the MPL can be an effective method to lower the hydrophobicity, but it reduces the binder force between the MPL and the substrate.[119] A way of improving fuel cell performance at both dry and humid conditions is the addition of a hydrophilic layer to the hydrophobic MPL.

Kitahara *et al.*[120–122] proposed a double MPL, in which a hydrophilic layer (polyvinyl alcohol (PVA) or TiO_2) was placed on top of the hydrophobic layer. The HL with TiO_2 was formed by 25 wt% TiO_2 as hygroscopic particles (size *ca.* 10 nm), 5 wt% silicone and carbon black. As can be seen in Fig. 16a, at low humidity an enhanced performance of the PEMFC with a double MPL, with either PVA or TiO_2, with respect to the fuel cell with a single-layer MPL was observed.[121] But at high humidity, the high hydrophilicity of the MPL with PVA causes flooding of the electrode, negatively affecting the performance of the PEMFC (Fig. 16b). Instead, an appropriate double MPL with TiO_2 is suitable to remove excess water from the cathode catalyst layer. A proper HF formed by 5% Nafion, 25% TiO_2 and carbon black further improved water removal from the catalyst layer.[122] A triple MPL, in which a TiO_2-containing HL hydrophilic layer was coated on a hydrophobic double MPL, was proposed to improve PEFC performance under both low and high humidity.[123] The triple MPL, in which the hydrophobic double MPL has had a gradient of hydrophobicity, obtained by different PTFE content, was more effectual to water removal from the cathode CL, resulting in a better fuel cell performance under high humidity than the double MPL. Wang *et al.*[124] fabricated a TiO_2 nanoarray (TiO_2NR) directly on the MPL of the GDL. The effect of TiO_2NR-coated MPL on the performance of PEMFC compared with that of the conventional GDL and TiO_2 nanoparticle-doped GDL is shown in Fig. 17. Under full wetting conditions (Fig. 17a), the performance of the cell with GDL-TiO_2NRs was close to that with conventional GDL, indicating that the incorporation of TiO_2NRs does not increase the ohmic resistance and does not reduce the catalyst activity. The performance of three PEMFCs under low-humidity conditions (21% RH) is shown in Fig. 17b. The addition of TiO_2 HL to the anode enhanced the performance of the cell at low relative humidity. The MPD of the PEMFC with GDL-TiO_2NRs was 1.3 times higher than that with GDL-TiO_2. The difference in the performance at low humidity of the PEMFCs with the HL was ascribed to GDL-TiO_2 limiting water retention capacity during fuel cell operation. Oh *et al.*[125] inserted an additional functional layer, formed by CNT sheets with Ti deposited onto them, between the CL and the MPL. This HL improves the PEMFC performance under all testing conditions (25–100% RH) due to their optimal pore structure and hydrophilic characteristics. The PEMFCs with the double layer showed up to ≈94% higher power density and ≈60% enhancement in charge transfer resistance than the cell with conventional GDL. A double-layer GDL with a hydrophilic TiO_2 layer was tested in low-humidification conditions.[126,127] Choun *et al.*[126] coated an ultrathin layer of hydrophilic TiO_2 on the hydrophobic MPL of GDL. By using TiO_2-coated GDL, a remarkable enhancement of PEMFC performance at low cathode humidification than that of the cell without TiO_2 was observed. Instead, to apply a hydrophilic layer on the MPL, Hou *et al.*[127] fabricated a modified GDL, in which a hydrophilic TiO_2 layer was placed between the hydrophobic layer and the GDB. This GDL was tested under low-humidity conditions and high PEMFC temperature. The performance of the single PEMFC with this modified GDL, used either in the anode, cathode, or both, was better than that of the cell using a GDL without the hydrophilic TiO_2 layer. Both these configurations, however, were not tested in high-humidity conditions. Finally, Wang *et al.*[128] fabricated a novel MPL-

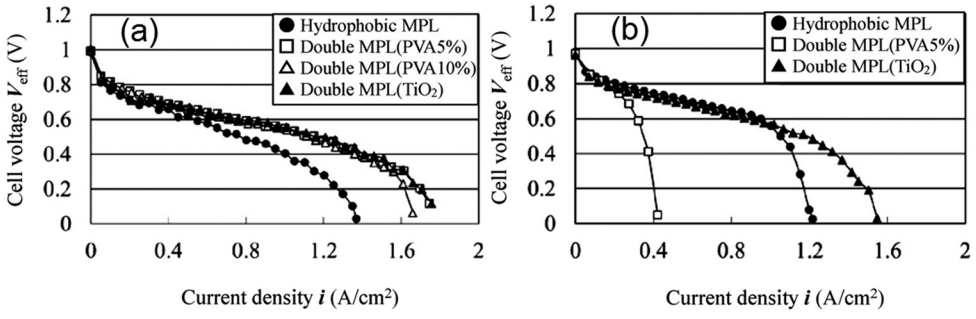

Fig. 16 (a) Influence of hydrophilic layer in double MPL-coated GDL (hydrophobic intermediate MPL: 20 mass% PTFE, d_m = 3 μm, h_{PTFE} = 90 μm) on PEFC performance under (a) low humidity (anode: 60% RH, cathode: 0% RH) and (b) high humidity (anode: 100% RH, cathode: 100% RH). Reproduced from ref. 121, copyright 2013, with permission from Elsevier.

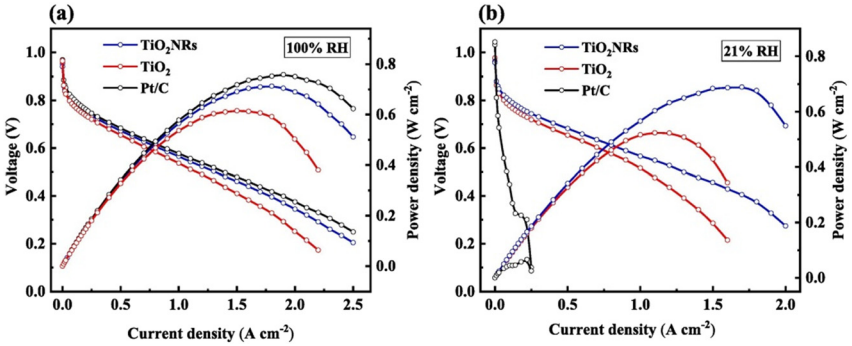

Fig. 17 Polarization and power density curves of PEMFCs with GDL-Pt/C, GDL-TiO_2 and GDL-TiO_2NRs as anode at 60 °C and (a) 100% RH, (b) 21% RH. Reproduced from ref. 124, copyright 2024, with permission from Elsevier.

coated GDB with hydrophobic and hydrophilic pores present in the same layer. This MPL, combining hydrophobic PVDF and Nafion with hydrophilic TiO_2 particles, remarkably decreased the oxygen transport resistance with respect to the hydrophobic MPL.

4. Conclusions and perspectives

Compared with graphite and other metals, titanium, although it is more expensive than stainless steel, has higher corrosion resistance, light weight and high strength. Its low density (*ca.* 60% than that of SS) allows reducing the mass and volume of bipolar plates. A drawback of titanium BPs is the poor formability at room temperature due to its low ductility and large springback. Commonly used manufacturing methods, such as stamping and rubber pad forming due to their ease of manufacturing and cost effectiveness, were used to fabricate Ti bipolar plates, but the results were not satisfactory. Therefore, new and cost-effective forming methods were explored to enhance Ti formability. Several novel methods were proposed to overcome the formability challenge of Ti bipolar plates, such as hot stamping, multistage stamping, electromagnetic forming and additive manufacturing. Multistage stamping and EMF seem to be the most promising methods in terms of channel depth and aspect ratio. Another drawback is the passivation film formed on the Ti surface, leading to a remarkable increase of the ICR. Moreover, F^- ions in the PEMFC environment can give rise to pitting corrosion, reducing PEMFC durability. These problems can be solved either by using Ti alloys as BP substrates or by coating the titanium surface with materials with high corrosion resistance and conductivity. Microalloying and low-alloying are widespread approaches to improve the corrosion resistance and ICR of titanium through utilization of limited but specific alloys. Alloying is a suitable method to enhance Ti corrosion resistance in F^--containing acidic solutions at low fluoride concentration. Titanium alloys, however, are still corroded at high fluoride concentrations. Therefore, future investigations should be directed towards the development of new alloys with increased corrosion resistance at high F^- concentrations. On the other hand, Ti-based ceramics, such as TiC and TiN, possessing high corrosion resistance and electrical conductivity, were proposed as low-cost coatings for Ti bipolar plates. The lower difference in thermal expansion coefficient between TiN and Ti than between TiC and Ti facilitates the formation of a tight TiN coating bound to Ti and decreases the stress between the coating and the substrate, making TiN more suitable than TiC as a coating for titanium BPs. Compared with the PVD method, PN is a cost-effective, simple, and promising method to modify the bipolar plate surface, avoiding the drawback of peeling of the coating owing to poor adhesion. PN of Ti, however, is commonly performed at high temperatures (≥900 °C), which overcome the α-Ti to β-Ti phase transformation temperature and can give rise to deformation of the treated workpiece. Furthermore, the cracks formed in the TiN film were attributed to the thermal expansion mismatch between TiN and Ti during cooling from high temperature. To overcome the drawbacks related to plasma nitriding at high temperatures, plasma nitriding at low temperature and different techniques other than plasma nitriding were utilized to coat titanium BPs with TiN layers. The MIP method, carried out at a temperature as low as only 250 °C, was used to fabricate TiN coating on Ti. A novel PVD technique, namely high-power impulse magnetron sputtering, was utilized to coat BP surfaces. The many advantages of this method, such as high coating density, good adhesion, higher hardness, and smooth surface, make it suitable for synthesizing TiN hard coatings. Beyond TiN, other compounds, such as TMN, TMC and carbon-based materials were tested as coatings for titanium BPs. All these coating showed high corrosion resistance and low ICR. The utilization of a-C as BP coatings, however, presents two drawbacks, that is, a weak coating–substrate bonding and coating detachment, owing to internal stress and permeation of corrosive media, related to the presence of pinholes, leading to substrate degradation. Effective methods to solve these problems are element doping and the use of multilayer structures. It is important to remark that, for the same coating the corrosion resistance can depend on the corrosion resistance of the substrate. Thus, to maximize the overall corrosion resistance, before the deposition of the coating, the corrosion resistance of the Ti

substrate should be maximized by Ti alloying and subsequent microstructural modification of the substrate surface.

Titanium has high strength, low density and outstanding corrosion resistance, so porous Ti is more suitable than carbon and stainless steel for use as gas diffusion backing. However, as in the case of BPs, the challenge is Ti manufacturing with proper porosity, thickness, and pore morphology. Moreover, the development of a low-cost titanium-based GDL manufacturing technology is a key factor for commercialization. Thus, the fabrication methods have to be thoroughly evaluated to make a suitable Ti GDB for PEMFC. Ti sinter, Ti fiber felt, and Ti foam were used as Ti GDB in PEMFCs, and various preparation methods such as freeze cast, micromachining and 3D printing were used to fabricate them.

While the internal resistances of the BP and GDL are small and can be ignored, the ICR between the BP and the GDL is relatively large and plays a key role in PEMFC performance. The ICR between BP and GDL depends on various parameters, such as manufacturing, substrate (bare or alloyed) and coating. The ICR of BP is commonly evaluated for a fixed GDL, overall carbon paper. As the ICR depends on the BP/GDL interface, ICR tests for a fixed BP should be performed using different GDLs. Supposedly, the ICR between uncoated Ti BPs or Ti-based coating and Ti GDB should be lower than that with carbon paper GDB. The results of the work of Luo *et al.*,[76] which compared the ICR of Ti (BP) with carbon paper (GDL) with that of Ti (BP) with Ti mesh (GDL) supports this assumption: the ICR of Ti/Ti mesh (7.69 mΩ cm^{-2}) was lower than that of Ti/carbon paper (23.70 mΩ cm^{-2}) (Fig. 18). Thus, for Ti bipolar plates, in the absence of coating, the use of a titanium GDL is advantageous compared to a carbon paper GDL.

Future studies should be addressed to the development of carbon-free integrated Ti-based BP/GDL systems formed by Ti BPs, either uncoated or coated by Ti compounds, and Ti GDL to evaluate their suitability for fuel cell application.

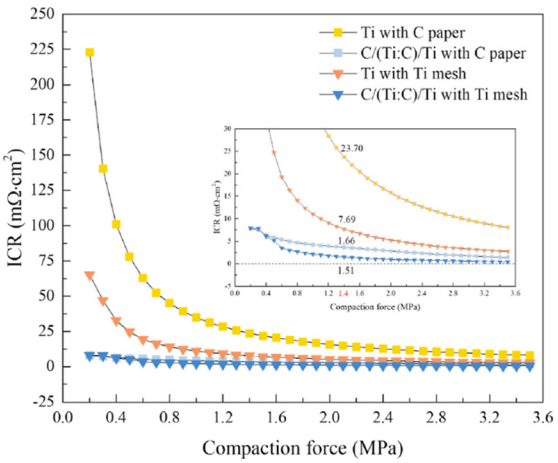

Fig. 18 ICR of bare Ti and C/(Ti : C)/Ti coated with GDLs (carbon paper and Ti mesh). Inset: low ICR values. Reproduced from ref. 76, copyright 2023, with permission from Elsevier.

Preliminary studies in this direction showed opposite results. An integrated BP/GDL Ti "bone" structure (*i*-BP-GDL) was fabricated by 3D printing.[115] Compared to the cell with conventional carbon-based GDL and BPs, the performance of the PEMFC with *i*-BP-GDL showed a considerable enhancement at high current densities. On the other hand, Kawachino *et al.*[116] integrated different PEMFC components into a single structure. Pt-decorated nanostructured Ti sheets were tested in a PEMFC as the catalyst, catalyst support, GDL and BP, but in this case the performance of the Pt/Ti system was lower than that of the Pt/C system.

Conflicts of interest

The author declares that there is no competing financial interest.

Abbreviations

ADT	Accelerated durability test
AM	Additive manufacturing
a-C	Amorphous carbon
AIP	Arc ion plating
BP	Bipolar plate
CL	Catalyst layer
CA	Contact angle
I_{corr}	Corrosion current density
DC	Direct current
DMLS	Direct metal laser sintering
DCS	Double cathode sputtering
DMFC	Direct methanol fuel cell
DSR	Differential speed rolling
ECAP	Equal channel angular pressing
EHF	Electrohydraulic forming
EMF	Electromagnetic forming
FF	Flow field
GDB	Gas diffusion backing
GDL	Gas diffusion layer
GO	Graphene oxide
HiPIMS	High power impulse magnetron sputtering
HL	Hydrophilic layer
HRDSR	High-ratio differential speed rolling
ICR	Interfacial contact resistance
MPS	Macroporous substrate
MPD	Maximum power density
MEA	Membrane electrode assembly
MPL	Microporous layer
MGO	Modified graphene oxide
MIP	Multi-arc ion plating
MS	Magnetron sputtering
OCV	Open circuit voltage
PVD	Physical vapor deposition
PN	Plasma nitriding
PANI	Polyaniline
PEMFC	Polymer electrolyte membrane fuel cell
PPy	Polypyrrole

RMS	Reactive magnetron sputtering
PE	Pulse electrodeposition
RT	Room temperature
RPF	Rubber pad forming
SS	Stainless steel
TMC	Transition metal carbide
TMN	Transition metal nitride
UFG	Ultrafine grained
UPA	Uniform pressure actuator

Data availability

No data were used in this article.

References

1 D. Shi, L. Cai, C. Zhang, D. Chen, Z. Pan, Z. Kang, Y. Liu and J. Zhang, Fabrication methods, structure design and durability analysis of advanced sealing materials in proton exchange membrane fuel cells, *Chem. Eng. J.*, 2023, **454**, 139995.
2 K. Yao, T. Long, Y. Wang, X.-Z. Yuan, Y. Yao and H. Wang, Measuring the through-plane and in-plane oxygen apparent diffusion coefficients in the gas diffusion layer, *Front. Energy Res.*, 2023, **11**, 1200603.
3 D. Park, S. Ham, Y.-J. Sohn, Y.-Y. Choi and M. Kim, Mass transfer characteristics according to flow field and gas diffusion layer of a PEMFC metallic bipolar plate for stationary applications, *Int. J. Hydrogen Energy*, 2023, **48**, 304–317.
4 R. Taspinar, S. Litster and E. C. Kumbur, A computational study to investigate the effects of the bipolar plate and gas diffusion layer interface in polymer electrolyte fuel cells, *Int. J. Hydrogen Energy*, 2015, **40**, 7124–7134.
5 M. Najafizadeh, S. Yazdi, M. Bozorg, M. Ghasempour-Mouziraji, M. Hosseinzadeh, M. Zarrabian and P. Cavaliere, Classification and applications of titanium and its alloys: A review, *J. Alloys Compd. Commun.*, 2024, **3**, 100019.
6 A. Hermann, T. Chaudhuri and P. Spagnol, Bipolar plates for PEM fuel cells: a review, *Int. J. Hydrogen Energy*, 2005, **30**, 1297–1302.
7 J. Liu, L. Zhang, B. Yuan, Y. Zhang, Z. Yang and J. Huang, Design and development of coating for metallic bipolar plates in proton exchange membrane fuel cell (PEMFC): A review, *Mater. Des.*, 2024, **246**, 113338.
8 N. F. Asri, T. Husaini, A. B. Sulong, E. H. Majlan and W. R. W. Daud, Coating of stainless steel and titanium bipolar plates for anticorrosion in PEMFC: A review, *Int. J. Hydrogen Energy*, 2017, **42**, 9135–9148.
9 P. Dong, Z. Li, S. Feng, Z. Wu, Q. Cao, L. Li, Q. Chen and X. Han, Fabrication of titanium bipolar plates for proton exchange membrane fuel cells by uniform pressure electromagnetic forming, *Int. J. Hydrogen Energy*, 2021, **46**, 38768–38781.
10 K. Karacan, S. Celik, S. Toros, M. Alkan and U. Aydin, Investigation of formability of metallic bipolar plates via stamping for light-weight PEM fuel cells, *Int. J. Hydrogen Energy*, 2020, **45**, 35149–35161.
11 F. K. Chen and K. H. Chiu, Stamping formability of pure titanium plates, *J. Mater. Process. Technol.*, 2005, **170**, 181–186.
12 S. Mahabunphachai, Ö. N. Cora and M. Koç, Effect of manufacturing processes on formability and surface topography of proton exchange membrane fuel cell metallic bipolar plates, *J. Power Sources*, 2010, **195**, 5269–5277.
13 M. J. Kim, C. K. Jin and C. G. Kang, The effect of different forming parameters on the depth of bipolar-plate channels in static-and dynamic-load stamping, *J. Eng. Manufact.*, 2015, **229**, 1976–1983.
14 N. Nakagaki, *SAE Technical Paper*, 2015, 2015-01-1174.
15 C. K. Jin, M. G. Jeong and C. G. Kang, Fabrication of titanium bipolar plates by rubber forming and performance of single cell using TiN-coated titanium bipolar plates, *Int. J. Hydrogen Energy*, 2014, **39**, 21480–21488.
16 K. H. Lee, C. K. Jin, G. Kang, H. Y. Seo and J. D. Kim, Fabrication of titanium bipolar plates by rubber forming process and evaluation characteristics of TiN coated titanium bipolar plates, *Fuel Cells*, 2015, **15**, 170–177.
17 V. Modanloo, V. Alimirzaloo and M. Elyasi, Manufacturing of titanium bipolar plates using warm stamping process, *Arab. J. Sci. Eng.*, 2020, **45**, 9661–9667.
18 Y. Wang, Q. Zhong, R. Hua, L. Cheng, C. Wang, H. He, F. Chen and Z. Ma, Ultrasonic vibration-assisted stamping of serpentine micro-channel for titanium bipolar plates used in proton-exchange membrane fuel cell, *Materials*, 2023, **16**, 3461.
19 G. Pang, D. Cai, H. Jiang, J. Cui, G. Li and Y. C. Lin, Mechanisms of strain rate effect on pure Ti deformation: Application in the bipolar plates forming process, *J. Mater. Process. Technol*, 2025, **342**, 118933.
20 Z. Xu, Z. Li, R. Zhang, T. Jiang and L. Peng, Fabrication of micro channels for titanium PEMFC bipolar plates by multistage forming process, *Int. J. Hydrogen Energy*, 2021, **46**, 11092–11103.
21 X. Zhang, N. Guo, Z. Hou, B. Chen, D. Yang, J. Min, P. Ming and C. Zhang, A novel multistage forming process with intermediate annealing for PEMFC titanium bipolar plates with fine flow channels, *Int. J. Hydrogen Energy*, 2024, **50**, 1362–1372.
22 Y. Xie, X. Fang, C. Wang, Q. Zhong, Y. Wang and R. Hua, Investigation into the three-stage formation of micro-channels with ultra-thin titanium sheets used for proton-exchange membrane fuel cell bipolar plates, *Materials*, 2024, **17**, 1071.
23 Q. Zhong, R. Hua, C. Wang, L. Cheng, Z. Ma, H. He and F. Chen, Investigation on three-stage stamping of micro-channels with titanium ultra-thin sheet used for PEM fuel cell bipolar plates, *Int. J. Adv. Manuf. Technol.*, 2023, **127**, 1377–1389.
24 Z. Zhang, Y. Wu, X. Hu, J. Guo, J. Yin, J. Yang, Z. Xiong and Y. Sun, Study on springback testing of ultra-thin titanium bipolar plates in stamping forming based on micro/mesoscopic scale effects, *J. Phys. Conf. Ser.*, 2025, **3104**, 012071.

25 J. Zhang, Z. Chen, H. Zhang, Y. Zeng, T. Hu and J. Tang, A new forming method of titanium bipolar plate for PEMFC: multi-step rolling forming, *J. Mater. Eng. Perform.*, 2025, **34**, DOI: 10.1007/s11665-025-12106-4.
26 V. Psyk, D. Risch, B. L. Kinsey, A. E. Tekkaya and M. Kleiner, Electromagnetic forming—A review, *J. Mater. Process. Technol*, 2011, **211**, 787–829.
27 F.-Q. Li, J. Zhao, J.-H. Mo, J.-J. Li and L. Huang, Comparative study of the microstructure of Ti-6Al-4V titanium alloy sheets under quasi-static and high-velocity bulging, *J. Mech. Sci. Technol.*, 2017, **31**, 1349–1356.
28 F.-Q. Li, J.-H. Mo, J.-J. Li, L. Huang and H.-Y. Zhou, Formability of Ti–6Al–4V titanium alloy sheet in magnetic pulse bulging, *Mater. Des.*, 2013, **62**, 337–344.
29 C. Zhu, J. Xu, H. Yu, D. Shan and B. Guo, Grain size effect on formability in electromagnetically assisted micro-bulging of pure titanium sheet, in *The Minerals, Metals & Materials Series*, ed. G. Daehn, J. Cao, B. Kinsey, E. Tekkaya, A. Vivek and Y. Yoshida, Springer, Cham, 2021.
30 M. Kamal and G. S. Daehn, A uniform pressure electromagnetic actuator for forming flat sheets, *J. Eng. Ind.*, 2007, **129**, 369–379.
31 H. M. Wang and Y. L. Wang, Investigation of bipolar plate forming with various die configurations by magnetic pulse method, *Metals*, 2019, **9**, 453.
32 Z. Wu, Q. Cao, J. Fu, Z. Li, Y. Wan, Q. Chen, L. Li and X. Han, An inner-field uniform pressure actuator with high performance and its application to titanium bipolar plate forming, *Int. J. Mach. Tools Manuf.*, 2020, **155**, 103570.
33 Q. Wang, J. Xu, S. Wang, Y. Zhao and Y. Wang, Analysis, simulation and experimental study of electromagnetic forming of titanium bipolar plate with arc-shaped uniform pressure coil, *Int. J. Mater. Form.*, 2024, **17**, 23.
34 C. Zhu, J. Xu, H. Yu, D. Shan and B. Guo, Hybrid forming process combining electromagnetic and quasi-static forming of ultra-thin titanium sheets: formability and mechanism, *Int. J. Mach. Tools Manuf.*, 2022, **180**, 103929.
35 Z. Wu, P. Dong, Y. Huang, Y. Chen, R. Liu, Q. Cao, L. Li, H. Wang, X. Han and Q. Wang, Formability and mechanism of ultra-thin titanium foil under the elevated temperature and high strain rate in electromagnetic forming, *J. Mater. Res. Technol.*, 2024, **31**, 2435–2449.
36 B. D. Gould, J. A. Rodgers, M. Schuette, K. Bethune, S. Louis, R. Rocheleau and K. Swider-Lyons, Performance and limitations of 3D-printed bipolar plates in fuel cells, *ECS J. Solid State Sci. Technol.*, 2015, **4**, P3063–P3068.
37 K. Swider-Lyons and B. D. Gould, Lightweight titanium metal bipolar plates for PEM fuel cells, *Mater. Sci. Forum*, 2016, **879**, 613–618.
38 H. Piri, X. T. Bi, H. Li and H. Wan, 3D-printed fuel-cell bipolar plates for evaluating flow-field performance, *Clean Energy*, 2020, **4**, 142–157.
39 S. Celik, B. Timurkutluk, U. Aydin and M. Yagiz, Development of titanium bipolar plates fabricated by additive manufacturing for PEM fuel cells in electric vehicles, *Int. J. Hydrogen Energy*, 2022, **47**, 37956–37966.
40 H. Heidary, M. de Lisi, M. M. Attallah, S. C. Cox, A. El-kharouf and R. Steinberg-Wilckens, Developing lightweight porous distributors for polymer electrolyte fuel cells via laser powder bed fusion, *J. Power Sources*, 2025, **656**, 238066.
41 S.-H. Wang, J. Peng and W.-B. Lui, Surface modification and development of titanium bipolar plates for PEM fuel cells, *J. Power Sources*, 2006, **160**, 485–489.
42 S.-H. Wang, J. Peng, W.-B. Lui and J.-S. Zhang, Performance of the gold-plated titanium bipolar plates for the light weight PEM fuel cells, *J. Power Sources*, 2006, **162**, 486–491.
43 J. Shi, P. Zhang, Y. Han, H. Wang, X. Wang, Y. Yu and J. Sun, Investigation on electrochemical behavior and surface conductivity of titanium carbide modified Ti bipolar plate of PEMFC, *Int. J. Hydrogen Energy*, 2020, **45**, 10050–10058.
44 J. Liu, F. Chen, Y. Chen and D. Zhang, Plasma nitrided titanium as a bipolar plate for proton exchange membrane fuel cell, *J. Power Sources*, 2009, **187**, 500–504.
45 P. Yi, C. Dong, T. Zhang, K. Xiao, Y. Ji, J. Wu and X. Li, Effect of plasma electrolytic nitriding on the corrosion behavior and interfacial contact resistance of titanium in the cathode environment of proton-exchange membrane fuel cells, *J. Power Sources*, 2019, **418**, 42–49.
46 H. Shen and L. Wang, Corrosion resistance and electrical conductivity of plasma nitrided titanium, *Int. J. Hydrogen Energy*, 2021, **46**, 11084–11091.
47 J. Jin, Z. He and X. Zhao, Formation of a protective TiN layer by liquid phase plasma electrolytic nitridation on Ti–6Al–4V bipolar plates for PEMFC, *Int. J. Hydrogen Energy*, 2020, **45**, 2489–12500.
48 Z. Yan, T. Li, Q. Wang, H. Li, Y. Wang, C. Wu, Y. Yan and Y. Chen, Surface conductivity and preferred orientation of TiN film for Ti bipolar plate, *Coatings*, 2022, **12**, 454.
49 D. Zhang, L. Duan, L. Guo, Z. Wang, J. Zhao, W.-H. Tuan and K. Niihara, TiN-coated titanium as the bipolar plate for PEMFC by multi-arc ion plating, *Int. J. Hydrogen Energy*, 2011, **36**, 9155–9161.
50 T. Li, Z. Yan, Z. Liu, Y. Yan and Y. Chen, Surface microstructure and performance of TiN monolayer film on titanium bipolar plate for PEMFC, *Int. J. Hydrogen Energy*, 2021, **46**, 31382–31390.
51 Z. Wang, B. Zhang, K. Gao and R. Liu, Adjustable TiN coatings deposited with HiPIMS on titanium bipolar plates for PEMFC, *Int. J. Hydrogen Energy*, 2022, **47**, 39215–39224.
52 J. Bi, J. Yang, X. Liu, D. Wang, Z. Yang, G. Liu and X. Wang, Development and evaluation of nitride coated titanium bipolar plates for PEM fuel cells, *Int. J. Hydrogen Energy*, 2021, **46**, 1144–1154.
53 E. Antolini, Transition metal nitrides: Essential and potential use in low-temperature fuel cells, *J. Electroanal. Chem.*, 2025, **979**, 118926.
54 W. Li, Y. Wang, X. Li, X. Zhou, L. Liu, X. Li, X. Jiang, C. Xiong, Y. Chen and F. You, Effect of N_2 ratio on the conductivity and corrosion resistance of TiN/TaN coating on TC4 bipolar plates for PEMFC, *Mater. Today Commun.*, 2025, **42**, 111415.

55 W. Li, Y. Wang, X. Li, X. Zhou, X. Jiang, C. Xiong, Y. Chen, F. You, Z. Guo, Y. Zhang, L. Liu and X. Li, Effect of Ti doping on properties of TiN/(Ta, Ti)N coated TC4 bipolar plate in proton exchange membrane fuel cells environment, *J. Power Sources*, 2025, **631**, 236227.
56 T. Li, H. Zhang, Y. Wang, C. Wu, Y. Yan and Y. Chen, TiCr transition layer promoting the growth of high-stability TiCrN coating for titanium bipolar plate, *Surf. Coat. Technol.*, 2022, **451**, 129026.
57 Y. Yan, H. Tao Li, Y. C. Zhang and T. Zhang, Lattice matching growth of high anti-corrosion TiCr/TiCrN coating for Ti bipolar plate, *J. Power Sources*, 2024, **614**, 235051.
58 W. Li, Y. Wang, X. Li, X. Zhou, X. Jiang, C. Xiong, Y. Chen, F. You, Z. Guo, Y. Zhang, L. Liu and X. Li, Effect of Ti doping on properties of TiN/(Ta, Ti)N coated TC4 bipolar plate in proton exchange membrane fuel cells environment, *J. Power Sources*, 2025, **631**, 236227.
59 P. Gao, Z. Xie, X. Wu, C. Ouyang, T. Lei, P. Yang, C. Liu, J. Wang, T. Ouyang and Q. Huang, Development of Ti bipolar plates with carbon/PTFE/TiN composites coating for PEMFCs, *Int. J. Hydrogen Energy*, 2018, **43**, 20947–20958.
60 P. Gao, Z. Xie, O. Chun, T. Tao, X. Wu and Q. Huang, Electrochemical characteristics and interfacial contact resistance of Ni-P/TiN/PTFE coatings on Ti bipolar plates, *J. Solid State Electrochem.*, 2018, **22**, 1971–1981.
61 Q. Yin, K. Zhang, X.-Z. Fu, X.-Z. Wang and J.-L. Kuo, Rapid coating preparation strategy for chromium nitride coated titanium bipolar plates of proton exchange membrane fuel cells, *Int. J. Hydrogen Energy*, 2022, **47**, 31434–31445.
62 L. Chen, R. Liu, B. Zhang, J. Lv and J. Zhang, Nano-Cr_2N dominated films with high conductivity and strong corrosion resistance for Ti bipolar plates, *Mater. Des.*, 2022, **224**, 111305.
63 B. Dang, Y. Han, K. Yang, D. Chen, M. Zhan, F. Ding, S. Li and P. Zhang, Effect of different N_2 partial pressures on the corrosion properties and conductivity of NbN_x coated titanium bipolar plates for PEMFCs, *Coatings*, 2025, **15**, 973.
64 J. Chen, S. Zhang, J. Zheng, Y. Dong, C. Zhang, J. Li, Z. Chen, J. Zhang and D. Sun, Excellent anti-corrosion and conductivity of NbN coated on Ti bipolar plate by controlling N_2 flow rates, *J. All. Comp.*, 2024, **976**, 173033.
65 L. Qin, G. Liang, J. Zhao, J. Kang and X. Zhang, Double glow plasma surface alloying with stepwise Cr/C doping: A robust pre-coating strategy for PEMFC Ti bipolar plates, *Mater. Lett.*, 2026, **402**, 139339.
66 Y. Gou, H. Chen, R. Li, J. Geng and Z. Shao, Nb–Cr–C coated titanium as bipolar plates for proton exchange membrane fuel cells, *J. Power Sources*, 2022, **520**, 230797.
67 Y. Chen, J. Xu, Z.-H. Xie and P. Munroe, Nanocrystalline TaCN coated titanium bipolar plate dedicated to proton exchange membrane fuel cell, *Ceram. Int.*, 2022, **48**, 19217–19231.
68 X. Zhang, Z. Wang, R. Wu, H. Jiang and J. Wang, Preparation and performance of graphene-doped indium tin oxide coatings on titanium bipolar plate surface, *Mater. Chem. Phys.*, 2024, **327**, 129833.
69 Y. Zhou, S. Tang, X. Sun, Y. Sun, Y. Pan, C. Deng, J. Hu, H. San and J. Han, Electrochemical properties and surface conductivity of Ti-Al coating on Ti-6Al-4V, *Appl. Surf. Sci.*, 2024, **654**, 159435.
70 S. Yuan, N. Lin, Q. Zeng, H. Zhang, X. Liu, Z. Wang and Y. Wu, Recent developments in research of double glow plasma surface alloying technology: a brief review, *J. Mater. Res. Technol.*, 2020, **9**, 6859–6882.
71 W. Li, L.-T. Liu, Z.-X. Li, Y.-F. Wang, H.-Z. Li and J.-J. Lei, Corrosion resistance and conductivity of amorphous carbon coated SS316L and TA2 bipolar plates in proton-exchange membrane fuel cells, *Diam. Relat. Mater.*, 2021, **118**, 108503.
72 Q. Meng, L. Yu, L. Shang, F. Wang, X. Liu and G. Zhang, Corrosive behavior and interfacial conductivity of stampable a-C film on titanium bipolar plate in proton exchange membrane fuel cells, *Diam. Relat. Mater.*, 2023, **135**, 109796.
73 L. Yu, L. Shang, G. Zhang, X. Li and Q. Meng, High-performance amorphous carbon films on titanium foils: Toward industrial preparation of coated metallic bipolar plates for proton exchange membrane fuel cells, *Int. J. Hydrogen Energy*, 2023, **48**, 34055–34066.
74 Z. Wang, J. Li, J. Lv and B. Zhang, Enhanced corrosion resistance of titanium bipolar plates for PEMFC by N/Ti co-doped a-C pseudo-multilayer coating, *Diam. Relat. Mater.*, 2025, **156**, 112463.
75 W. Yan, Y. Zhang, L. Chen, J. Luo, P. Pang, X. Zhang, B. Liao and M. Ying, Corrosion behavior and interfacial conductivity of amorphous hydrogenated carbon and titanium carbide composite (a-C: H/TiC) films prepared on titanium bipolar plates in PEMFCs, *Diam. Relat. Mater.*, 2021, **120**, 108628.
76 X. Luo, L. Chang, C. Ren, J. Zhang, D. Zhang, J. Yao, J. Song, Z. Deng, C. Dong and X. Li, Sandwich-like functional design of C/(Ti:C)/Ti modified Ti bipolar plates for proton exchange membrane fuel cells, *J. Power Sources*, 2023, **585**, 233633.
77 Y. Gou, G. Jiang, J. Geng and Z. Shao, Properties of NbC/a-C:H films on titanium bipolar plates for proton exchange membrane fuel cells, *Fuel Cells*, 2023, **23**, 51–59.
78 V. E. Pukha, A. A. Glukhov, A. A. Belmesov, E. N. Kabachkov, I. I. Hhodos, M. Khadem, D.-E. Kim and P. A. Karaseov, Corrosion-resistant nanostructured carbon-based coatings for applications in fuel cells based on bipolar plates, *Vacuum*, 2023, **218**, 112643.
79 J. Wang, L. Min, F. Fang, W. Zhang and Y. Wang, Electrodeposition of graphene nano-thick coating for highly enhanced performance of titanium bipolar plates in fuel cells, *Int. J. Hydrogen Energy*, 2019, **44**, 16909–16917.
80 Y. Liu, L. Min, W. Zhang and Y. Wang, High-performance graphene coating on titanium bipolar plates in fuel cells via cathodic electrophoretic deposition, *Coatings*, 2021, **11**, 437.

81 F. Yu, K. Wang, L. Cui, S. Wang, M. Hou, F. Xiong, R. Zou, P. Gao, H. Peng and Z. Liu, Vertical-graphene-reinforced titanium alloy bipolar plates in fuel cells, *Adv. Mater.*, 2022, **34**, 2110565.
82 H. K. Hwang and S. J. Kim, Accelerated corrosion and electrochemical characteristics of carbon-coated titanium bipolar plates by doctor-blade technology for PEMFC, *npj Mater. Degrad.*, 2025, **9**, 105.
83 Y. Wang and D. O. Northwood, Effect of substrate material on the corrosion of TiN-coated stainless steels in simulated anode and cathode environments of proton exchange membrane fuel cells, *J. Power Sources*, 2009, **191**, 483–488.
84 A. Balyanov, J. Kutnyakova, N. A. Amirkhanova, V. V. Stolyarov, R. Z. Valiev, X. Z. Liao, Y. H. Zhao, Y. B. Jiang, H. F. Xu, T. C. Lowe and Y. T. Zhu, Corrosion resistance of ultrafine-grained Ti, *Scr. Mater.*, 2004, **51**, 225–229.
85 H. S. Kim, S. J. Yoo, J. W. Ahn, D. H. Kim and W. J. Kim, Ultrafine grained titanium sheets with high strength and high corrosion resistance, *Mater. Sci. Eng., A*, 2011, **528**, 8479–8485.
86 Q. Liu, X. Wang, D. Yin and X. Zhang, Mechanical properties, corrosion resistance, and rubber pad forming of cold differential speed-rolled pure titanium for bipolar plates of proton-exchange membrane fuel cells, *Int. J. Hydrogen Energy*, 2022, **47**, 17737–17748.
87 G. Krállics, J. Gubicza, Z. Bezi and I. Barkai, Manufacturing of ultrafine-grained titanium by caliber rolling in the laboratory and in industry, *J. Mater. Process. Technol.*, 2014, **214**, 1307–1315.
88 K. Shliakhetka, I. Pohrelyuk, S. Sheykin, S. Lavrys, M. Balog and K. Kamyshnykova, Corrosion protection of highly porous titanium by surface engineering, *Surf. Coat. Technol.*, 2024, **482**, 130663.
89 H. S. Kim and W. J. Kim, Annealing effects on the corrosion resistance of ultrafine-grained pure titanium, *Corros. Sci.*, 2014, **89**, 331–337.
90 H. Zhu, X. Wang, W. Meng, P. Ming and F. Kong, Effect of annealing time on microstructure and properties of Ti-Nb-Ni sheets as bipolar plates substrates, *Int. J. Hydrogen Energy*, 2024, **57**, 1263–1272.
91 Z. B. Wang, H. X. Hu, Y. G. Zheng, W. Ke and Y. X. Qiao, Comparison of the corrosion behavior of pure titanium and its alloys in fluoride-containing sulfuric acid, *Corros. Sci.*, 2016, **103**, 50–65.
92 N. Aukland, A. Boudina, D. S. Eddy, J. V. Mantese, M. P. Thompson and S. S. Wang, Alloys that form conductive and passivating oxides for proton exchange membrane fuel cell bipolar plates, *J. Mater. Res.*, 2004, **19**, 1723–1729.
93 F. A. Bonilla, T. S. Ong, P. Skeldon, G. E. Thompson, J. Piekoszewski, A. G. Chmielewski, B. Sartowska and J. Stanislawski, Enhanced corrosion resistance of titanium foil from nickel, nickel-molybdenum and palladium surface alloying by high intensity pulsed plasmas, *Corros. Sci.*, 2003, **45**, 403–412.
94 H. Zhu, X. Wang, W. Meng, P. Ming and F. Kong, Corrosion behavior of Ti-Nb-Ni foil as bipolar plates substrate in simulated PEMFC solution: Effects of fluoride concentration and temperature, *Fuel*, 2024, **362**, 130823.
95 M. Song, Q. Wang and C. Dong, Ti-Al-Ta alloy for fuel cell bipolar plates with low contact resistance, *J. Mater. Eng.*, 2024, **52**, 80–90.
96 Z. Yuan, H. Chu, Y. Pan, F. Li, X. Wang, L. Li, P. Hu, B. Du and M. D. Hayat, Enhanced conductivity behavior of titanium-based bipolar plate oxide films through microalloying, First-principles calculations and experimental investigations, *Ceram. Int.*, 2024, **50**, 4101–4108.
97 M. Stancheva and M. Bojinov, Influence of fluoride content on the barrier layer formation and titanium dissolution in ethylene glycol-water electrolytes, *Electrochim. Acta*, 2012, **78**, 65–74.
98 Z. B. Wang, H. X. Hu, C. B. Liu and Y. G. Zheng, The effect of fluoride ions on the corrosion behavior of pure titanium in 0.05 M sulfuric acid, *Electrochim. Acta*, 2014, **135**, 526–535.
99 M. Nakagawa, S. Matsuya and K. Udoh, Corrosion behavior of pure titanium and titanium alloys in fluoride-containing solutions, *Dent. Mater. J.*, 2001, **20**, 305–314.
100 X. Wang, Y. Pan, J. Yang, R. Zhu, Y. Zhou, Z. Yuan, H. Chu, P. Hu and L. Li, Corrosion behavior of Ti-0.3Mo-0.8Ni (TA10) alloy in proton exchange membrane fuel cell environment: Experimental and theoretical studies, *Int. J. Electrochem. Sci.*, 2023, **18**, 100239.
101 Y. Li, X. Wang, Y. Li, Z. He, G. Zhang, Z. Wang, S. Wang, F. Hu and Q. Zhou, Corrosion and interfacial contact resistance of NiTi alloy as a promising bipolar plate for PEMFC, *Molecules*, 2024, **29**, 3696.
102 S. Park, J.-W. Lee and B. N. Popov, A review of gas diffusion layer in PEM fuel cells: Materials and designs, *Int. J. Hydrogen Energy*, 2012, **37**, 5850–5865.
103 Q. Chen, Z. Niu, H. Li, K. Jiao and Y. Wang, Recent progress of gas diffusion layer in proton exchange membrane fuel cell: Two-phase flow and material properties, *Int. J. Hydrogen Energy*, 2021, **46**, 8640–8671.
104 F. C. Lee, M. S. Ismail, D. B. Ingham, K. J. Hughes, L. Ma, S. M. Lyth and M. Pourkashanian, Alternative architectures and materials for PEMFC gas diffusion layers: A review and outlook, *Renew. Sustain. Energy Rev.*, 2022, **166**, 112640.
105 J. Hussain, D.-K. Kim, S. Park, M.-W. Khalid, S.-S. Hussain, B. Lee, M. Song and T.-S. Kim, Porous material (titanium gas diffusion layer) in proton exchange membrane fuel cell/electrolyzer: Fabrication methods & geodict. A critical review, *Materials*, 2023, **16**, 4515.
106 C. M. Hwang, M. Ishida, H. Ito, T. Maeda, A. Nakano, Y. Hasegawa, N. Yokoi, A. Kato and T. Yoshida, Influence of properties of gas diffusion layers on the performance of polymer electrolyte-based unitized reversible fuel cells, *Int. J. Hydrogen Energy*, 2011, **36**, 1740–1753.
107 Y. Wang, D. Y. C. Leung, J. Xuan and H. Wang, A review on unitized regenerative fuel cell technologies, part-A: Unitized regenerative proton exchange membrane fuel cell, *Renew. Sustain. Energy Rev.*, 2016, **65**, 961–977.

108 S. Wang, A. Z. Weber and X. Peng, Advances and prospects to achieve high-performing and durable proton-exchange-membrane unitized regenerative fuel cells, *Curr. Opin. Electrochem.*, 2023, **40**, 101340.
109 T. Hottinen, M. Mikkola, T. Mennola and P. Lund, Titanium sinter as gas diffusion backing in PEMFC, *J. Power Sources*, 2003, **118**, 183–188.
110 H. Moydien, P. Levecque and D. Susac, Experimental study of water management and performance of titanium fiber felts as versatile gas diffusions layers for PEMFCs, *Int. J. Hydrogen Energy*, 2023, **48**, 32968–32981.
111 T. Ma, H. Guo, Z. Gu, W. Lin, J. Qi, C. Yu and J. Li, Performance analysis and experimental study of titanium GDL in proton exchange membrane fuel cell, *Int. J. Hydrogen Energy*, 2024, **83**, 604–613.
112 H. Choi, O.-H. Kim, M. Kim, H. Choe, Y.-H. Cho and Y.-E. Sung, Next-generation polymer-electrolyte-membrane fuel cells using titanium foam as gas diffusion laye, *ACS Appl. Mater. Interfaces*, 2014, **6**, 7665–7671.
113 K. Fushinobu, D. Takahashi and K. Okazaki, Micromachined metallic thin films for the gas diffusion layer of PEFCs, *J. Power Sources*, 2006, **158**, 1240–1245.
114 A. Jayakumar, S. Singamneni, M. Ramos, A. M. Al-Jumaily and S. S. Pethaiah, Manufacturing the gas diffusion layer for PEM fuel cell using a novel 3D printing technique and critical assessment of the challenges encountered, *Materials*, 2017, **10**, 796.
115 X. Wang, H. Ma, H. Peng, Y. Wang, G. Wang, L. Xiao, J. Lu and L. Zhuang, Enhanced mass transport and water management of polymer electrolyte fuel cells via 3-D printed architectures, *J. Power Sources*, 2021, **515**, 230636.
116 D. Kawachino, M. Yasutake, Z. Noda, J. Matsuda, S. M. Lyth, A. Hayashi and K. Sasaki, Surface-modified titanium fibers as durable carbon-free platinum catalyst supports for polymer electrolyte fuel cells, *J. Electrochem. Soc.*, 2020, **167**, 104513.
117 T. Tanuma, M. Kawamoto and S. Kinoshita, Effect of properties of hydrophilic microporous layer (MPL) on PEFC performance, *J. Electrochem. Soc.*, 2017, **164**, F499–F505.
118 R. Omrani and B. Shabani, Gas diffusion layer modifications and treatments for improving the performance of proton exchange membrane fuel cells and electrolysers: A review, *Int. J. Hydrogen Energy*, 2017, **47**, 28515–28536.
119 T. Kitahara, T. Konomi and H. Nakajima, Microporous layer coated gas diffusion layers for enhanced performance of polymer electrolyte fuel cells, *J. Power Sources*, 2010, **195**, 2202–2211.
120 T. Kitahara, H. Nakajima and K. Mori, Hydrophilic and hydrophobic double microporous layer coated gas diffusion layer for enhancing performance of polymer electrolyte fuel cells under no-humidification at the cathode, *J. Power Sources*, 2012, **199**, 29–36.
121 T. Kitahara, H. Nakajima, M. Inamoto and M. Morishita, Novel hydrophilic and hydrophobic double microporous layer coated gas diffusion layer to enhance performance of polymer electrolyte fuel cells under both low and high humidity, *J. Power Sources*, 2013, **234**, 129–138.
122 P. Wang, H. Nakajima and T. Kitahara, Effect of hydrophilic layer in double microporous layer coated gas diffusion layer on performance of a polymer electrolyte fuel cell, *J. Electrochem. Soc.*, 2023, **170**, 124514.
123 T. Kitahara, H. Nakajima, M. Inamoto and K. Shinto, Triple microporous layer coated gas diffusion layer for performance enhancement of polymer electrolyte fuel cells under both low and high humidity conditions, *J. Power Sources*, 2014, **248**, 1256–1263.
124 Y. Wang, W. Zhang, H. Liu, Q. Xu, L. Khotseng, Y. Cheng and H. Su, Cultivating titanium dioxide nanoarrays on gas diffusion layer for advancing self-humidifying proton exchange membrane fuel cell, *Fuel*, 2024, **366**, 131322.
125 H. Oh, J. Park, G. Park, J. Baek, J. Youn, S. Yang, J. Na, D. Kim, J. Lim, H. Lee, Y. Jeong and T. Park, Design strategies for high performance of proton exchange fuel cells with Ti-sputtered carbon nanotube sheet functional layer, *Adv. Funct. Mater.*, 2025, **35**, 2412311.
126 M. Choun, S. Chung, H. Jeon, S. Uhm and J. Lee, Atomic-layer-deposited TiO_2 on cathode gas diffusion layer for low humidity operation in hydrogen fuel cells, *Electrochem. Commun.*, 2012, **24**, 108–111.
127 S. Hou, Y. Ye, S. Liao, J. Ren, H. Wang, P. Yang, K. Du, J. Li and H. Peng, Enhanced low-humidity performance in a proton exchange membrane fuel cell by developing a novel hydrophilic gas diffusion layer, *Int. J. Hydrogen Energy*, 2020, **45**, 937–944.
128 P. Wang, H. Nakajima and T. Kitahara, Hydrophilic and hydrophobic composite microporous layer coated gas diffusion layers for performance enhancement of polymer electrolyte fuel cells, *J. Electrochem. Soc.*, 2024, **171**, 014501.